Nondestructive Evaluation of Wood Products

19

Robert J. Ross, Xiping Wang, and Christopher Adam Senalik

Contents

Abstract

The field of nondestructive evaluation (NDE) of materials is constantly evolving. This is especially true in the area of wood and fiber-based materials. A significant effort has been devoted toward the discovery and development of NDE technologies for use with wood-based products. Today, research and technology transfer efforts are underway throughout the world to further the development and use of nondestructive methods to address the many challenges that arise with using forest resources. Efforts are underway that span a broad spectrum of utilization and technology issues from those that focus on the use of previously developed techniques for solving utilization issues with plantation wood to the use of NDE techniques in the assessment of historic artifacts and structures.

The objective of this chapter is to provide scientific and technical information on several techniques that are used to nondestructively evaluate wood and wood-based products. This includes near infrared, optical, acoustic, transverse vibration, static bending, proof loading, as well as piezoelectric-based techniques. The techniques presented in this chapter have a solid technical base, with published research findings on their discovery and use dating to the middle of the twentieth century. The underlying science for each technique is presented, followed by a summary of published research findings on its use for nondestructively evaluating wood products.

Keywords

Nondestructive testing · Wood properties · Wood defects · Near infrared · Optical scanning · Acoustic testing · Transverse vibration · Static bending · Proof loading · Piezoelectric technique

19.1 Fundamental Concepts and Historical Context

Nondestructive evaluation (NDE) is the science of identifying the physical and mechanical properties of a piece of material without altering its end-use capabilities and then using this information to make decisions regarding appropriate applications. Such evaluations rely upon nondestructive testing (NDT) technologies to provide accurate information pertaining to the properties, performance, or condition of the material in question.

R. J. Ross (✉) · X. Wang · C. A. Senalik
USDA Forest Service, Forest Products Laboratory, Madison, WI, USA
e-mail: robert.j.ross@usda.gov; xiping.wang@usda.gov; christopher.a.senalik@usda.gov

P. Niemz et al. (eds.), *Springer Handbook of Wood Science and Technology*,
https://doi.org/10.1007/978-3-030-81315-4_19

Nondestructive evaluation of wood

Evaluation of visual characteristics
Color
Presence of defects

Mechanical tests
Flexural stiffness
Proof loading
- Bending
- Tension
- Compression

Probes/coring

Physical tests
Electrical properties
Vibrational properties
Wave propagation
Acoustic emissions

Chemical tests
Composition
Presence of treatments
- Preservatives
- Fire retardants

Fig. 19.1 Nondestructive testing techniques

Fig. 19.2 A late eighteenth-century Hudson Bay Company York boat

Many tests or techniques can be categorized as nondestructive (Fig. 19.1). A variety of tests can be performed on a material or product, with selection of the appropriate test dictated by the particular performance or quality characteristic of interest. Evaluation of visual characteristics of sawn timber is probably one of the most widely used nondestructive techniques in the forest products industry. Characteristics such as the size, number, and location of knots are common visual characteristics considered when grading both structural and nonstructural sawn timber.

One of the first uses of a nonvisual nondestructive testing method involved a procedure to evaluate timbers for boats used by the Hudson Bay Company, Canada, in the late eighteenth century (Fig. 19.2):

> "A York boat, which took two skilled men only two weeks to build, would last three seasons with minimum maintenance. The trickiest part of the construction process was to find the proper piece of spruce or tamarack for a seaworthy keel. Samples were tested by being placed on stocks and a pocket watch held against the butt at one end. The builder listened for the tick at the other. Only if the ticking resonated loudly and clearly through the wood was it judged suitable to withstand the stresses of being carved into a keel." From *Caesars of the Wilderness: Company of Adventures, Volume II,* by Peter C. Newman [1].

The field of nondestructive evaluation (NDE) of materials is constantly evolving. This is especially true in the area of wood and fiber-based materials. For example, early research on NDE technologies for wood products focused on methods for assessing the performance characteristics of structural lumber in North America. Nondestructive testing techniques, equipment, and evaluation procedures that resulted from those efforts are now in widespread use. Currently, worldwide research and development efforts are under way to examine potential use of a wide range of nondestructive technologies for evaluating wood and wood-based materials – from seedlings to in-place structures.

The original impetus for research in NDE of wood was the need to provide methodologies for assessing wood-based materials and products so that more accurate decisions could be made about proper use. This remains the major driving force for NDE of wood, with two significant additional challenges. First is an increased emphasis around the world to address forest and ecosystem health issues. Utilization of woody biomass from widely varying growing conditions will play a key role in providing economical options for managing the health of these forests and ecosystems. Second, the marketplace has become global in nature. Shipments of raw materials and products between countries on different continents are now commonplace. All these challenges require accurate, cost-effective NDE technologies.

While this chapter focuses upon foundational research primarily from the United States and Canada, it is important to note that study of NDT of wood is conducted worldwide. For several decades, advancements in the field have come from scientists across dozens of countries through investigations both local and global in scope.

Since the early 1960s, an international research community has conducted NDE research to provide the technologies needed to address these challenges. This community meets at various sites around the world to discuss results of their efforts at the International Nondestructive Testing and Evaluation of Wood Symposium. Initiated in 1963, this symposium has been a source of technical information on the discovery, development, and use of nondestructive technologies for wood materials for over 50 years. Proceedings from each meeting are prepared, published, and made available [2–4, 5]. Many of the key topical areas presented and discussed in these meetings are summarized in Ross [6].

The objective of this chapter is to provide scientific and technical information on several techniques that are used to nondestructively evaluate wood and wood-based products. This includes near infrared, optical, acoustic, transverse vibration, static bending, proof loading, as well as piezoelectric-based techniques. This chapter does not provide a review of every technique that has been investigated for nondestructive evaluation of wood-based materials. The techniques presented in this chapter have a solid technical base, with published research findings on their discovery and use dating to the middle of the twentieth century. The underlying science for each technique is presented, followed by a summary of published research findings on its use for nondestructively evaluating wood products.

19.2 Near-Infrared and Optical Techniques

19.2.1 Near-Infrared Techniques

Near-infrared (NIR) spectroscopy is a spectroscopic method that uses the NIR region of the electromagnetic spectrum. NIR spectroscopy involves measurement of the wavelength and intensity of absorption of NIR light by a specific material. Originally developed for use in biomedical applications, this technique has been thoroughly investigated for use in the forest products industry, with potential applications in wood quality monitoring, wood composites manufacturing, and monitoring of the deterioration of wood. A review of the science and baseline research has been prepared by So et al. [7].

NIR spectroscopy can be used to measure the stiffness of increment cores with acceptable accuracy [8, 9]. Meder et al. [10] conducted a study that involved the scanning, processing, and tracking of 180 radiata pine cants. The cants were scanned on the surface and then broken down into individual pieces of sawn timber. The NIR spectra were found sensitive to surface properties of the cant, which made prediction of sawn-timber stiffness possible but somewhat variable. The results of this study suggest that NIR technology can be used to estimate the value of sawn timber from cants, but it is perhaps more suited for smaller dimension sawn timber because only the absorbance at the surface can be measured. This and other work showed that the mechanical properties of wood could be predicted even when the moisture content of the wood varied over a wide range [10–12].

NIR spectroscopy can be used to determine the stiffness of radiata pine veneers [13]. Testing of small laminated veneer lumber (LVL) samples made from NIR-graded veneers was performed for calibration purposes, and the results showed the potential for NIR spectroscopy as a tool for stiffness evaluation prior to lay-up of plywood and LVL panels.

Kelley et al. [14] first reported on the use of these techniques to monitor decay in wood and the mechanical properties of treated wood and wood that has been exposed to decay organisms [15, 16].

Laboratory work aimed at quantifying the biodegradation process of wood during exposure to natural weathering using NIR techniques was investigated by Wang et al. [17]. Approximately 330 specimens of southern pine sawn timber were placed “above-ground” at an outdoor exposure site near Gulfport, Mississippi, USA, for periods up to five years. Additional 90 specimens were stored indoors to serve as controls. Two chemical preservative treatments, CCA and DDAC, were also applied to several sets of sawn-timber specimens. NIR spectroscopy techniques were used to characterize the condition of the weathered wood surface. Multivariate statistical tools were used to further analyze data from the NIR spectra. Results indicated that NIR spectral analysis, in conjunction with multivariate statistical analysis, had good potential for monitoring changing surface conditions of wood structural members subjected to natural weathering.

19.2.2 Optical Scanning Techniques

Optical information on wood surfaces is central to many wood processing decisions, from assessing overall wood quality to locating specific defects such as knots, checks, splits, holes, wane, pitch streak, and grain pattern. Substantial efforts have been made to develop automated scanning systems to detect defects in various wood products based on optical data collected from wood surfaces. Optical methods that have been investigated include the use of black and white cameras, color cameras, and spectrometers to measure intensity and color of reflected light. In addition, laser-scanning methods have emerged as powerful and economical means of determining the size, shape, and features of wood and quickly gained acceptance in the wood industry.

Camera System

Color information can be valuable for detecting and classifying surface defects in wood, but its usefulness depends on the color data format and the analysis technique used. Early applications of machine vision in the wood processing industry tend to be relatively simple. They work with binary or grayscale images and ignore the intricacies of human vision, especially its ability to perceive color. This simplifies system design and reduces the amount of data to be manipulated [18]. Conners et al. [19, 20] extended their work with grayscale vision systems by reviewing the literature related to wood color and how color might be used with machine vision [21]. Their work also included some experiments with a grayscale system and color filters to determine the effect of adding color information to their defect-classifying

algorithm. They reported that using only the red and blue data was nearly as effective as using the red, green, blue, and brightness data. Forrer et al. [22, 23] also used color data with a number of sweep-and-mark algorithms to identify likely defect areas in images of Douglas-fir (*Pseudotsuga menziesii*) veneer. For loose and tight knots, open holes, and pitch pockets/streaks, the statistical algorithm generally produced better results than either the morphological or color-cluster algorithms. It achieved an overall 99.0% accuracy in correctly identifying tiles containing knots and open holes, while maintaining an overall 85.5% accuracy in detecting clear wood. In a study to investigate color spaces for detecting defects in Douglas-fir veneer, Brunner et al. [24] confirmed that only two color parameters are required to separate defects from clear wood – one measuring brightness and one chromaticity. They further concluded that there is no benefit in mathematically transforming the initial National Television Standards Committee red, green, and blue (RGB) image data because the original R and B parameters are sufficient for detecting common defects in Douglas-fir.

Examples of current optical scanning methods in the forest products industry include the use of color line scan cameras for automatic optimized crosscutting [25] and the use of color information in sorting red oak edge-glued panel parts for improved panel uniformity [26, 27].

Laser Scanning System

Laser scanning is most commonly used in several aspects of sawn-timber production and quality assessment in both hardwood and softwood logs [28]. The key components of a laser scanning system are a laser line generator and a camera. Laser scanner design has several variations. Some have multiple laser beams and a single camera, whereas other scanners have two cameras and a single laser. Most scanners use lasers in the visible spectrum that must operate out of direct sunlight.

The camera and laser are separated by a measured distance and the camera is aimed toward the laser line at a specific angle. Using the camera angle, distance between camera and laser, and triangulation, the distance of points along the laser line projected on an object can be determined. Figure 19.3 shows the mechanics of projecting a point from the laser line onto the camera's image plane. Processing the location of points on the laser line onto the camera's image plane allows the shape and size of an object to be calibrated.

Sawn-timber scanning: Fig. 19.4 shows a typical configuration of a laser scanner in a sawmill. This scanning system consists of two laser scanners that capture two distinct data types – profile scanning data and tracheid effect data. The profile scanner on the right aims at the board at a shallow angle and is primarily used to provide accurate measurements

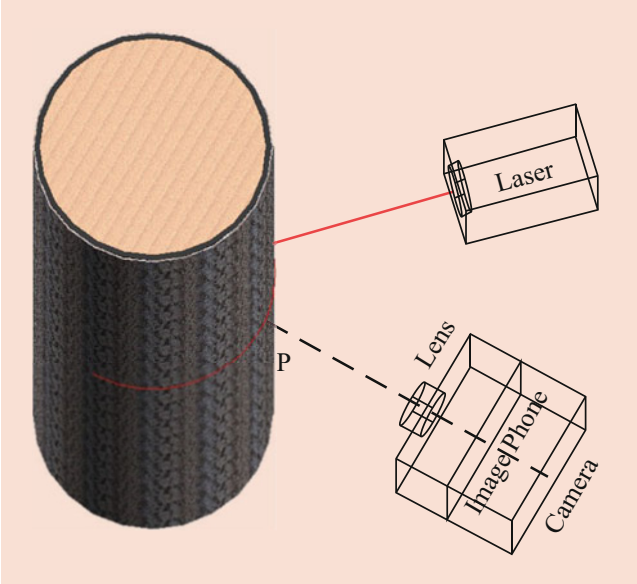

Fig. 19.3 Diagram of scanning head showing laser, camera, and image plane [28]

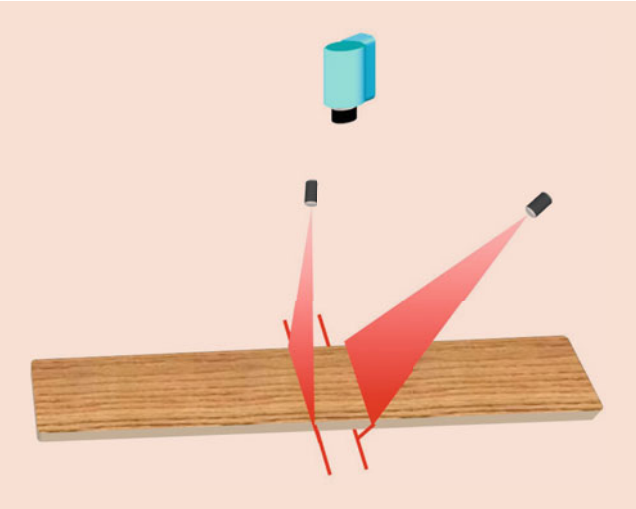

Fig. 19.4 Diagram of laser scanner used in a sawmill [28]

of the amount of wane, void, and sawn-timber width, and the distance between two edges with wane. Sawn-timber profile data are subsequently used to automate the edging and trimming of sawn timber to produce maximum grade and value [29].

The laser scanner aimed at the sawn timber at a perpendicular angle is used to scan for the tracheid effect data that are subsequently used to determine the angle of wood grain along the length of the sawn timber. When a laser beam is projected onto the surface of wood, the beam is mainly spread along the fibers, called tracheid in softwood, giving an elliptical spot extended in the orientation of the fibers. This phenomenon is commonly referred to as the tracheid effect.

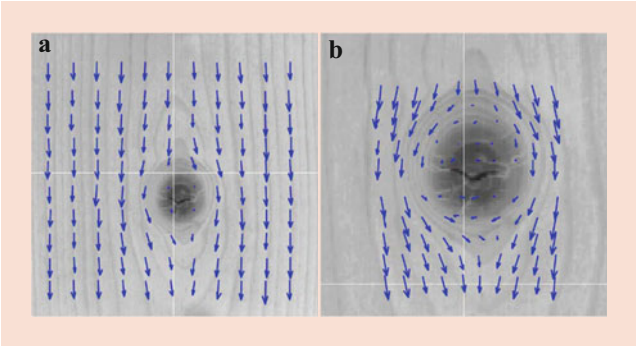

Fig. 19.5 Vector field showing the measured fiber orientation around a small knot on a spruce surface. (**a**) Image covering 60x60 mm^2. (**b**) Close-up of the same surface as image a covering 30x30 mm^2. The vector length is a measure of the eccentricity of the scattered light (i.e. the validity of the measurement) [30]

Figure 19.5 shows an example of tracheid effect for a small knot on a spruce surface. The measured grain orientation was plotted by a vector field overlaid onto an image of the surface. The angle of glow of the laser beam along the wood surface shows the angle of the wood grain. Thus, the angle of the wood grain around defects such as knots, pitch pockets, decay, and compression wood can be detected and used as indicators for defects [30–34]. The tracheid scanning technology was first used commercially to locate defects in hardwoods and softwoods for the production of furniture and moldings, but its use has since expanded. Today, several manufacturers produce commercial laser-scanning equipment capable of tracheid effect scanning [28].

Log scanning: The use of laser-scanning systems has also been extended to softwood and hardwood logs for determining diameter, shape, length, sweep, and taper of logs before processing. The scanning data are then used to optimize the sawing pattern. A typical method of laser scanning a log is to pass the log through an array of three to four laser scanning heads arranged around the log. Typically, the logs are on a chain and are passed through the scanner. During laser scanning, a series of scan lines are projected around the circumference of the log along its length. The resolution of the scanning system is the distance between the scan lines. The shorter the distance between the scan lines, the higher the resolution. The resolution of a log laser scanning system is normally between 15 and 60 cm, although much higher resolutions are possible. The higher the resolution, the greater the detail captured about the log and the greater the amount of data that must be processed. The log images shown in Fig. 19.6 are high-resolution scans of yellow-poplar (*Liriodendron tulipifera*) logs at a resolution of 1.6 mm. This scan is from an experimental scanner developed by the Forest Service [35]. In the scan imagery, defects in the image and log shape are easily discerned.

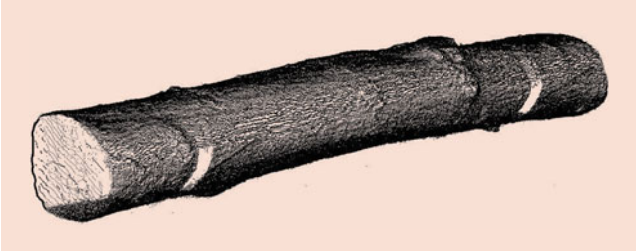

Fig. 19.6 High-resolution 3D scan of a hardwood log [35]

Methods have been developed for automated detection of severe defects on hardwood log surfaces using laser scan data [35, 36]. These methods use parallel processing and contour analysis approaches to detect bumps and depressions associated with severe surface defects. In addition, these methods can grade the log to Forest Service log grades, and the potential grade recovery of the log can be determined using the yield tables developed by Hanks et al. [37]. In addition, models have been developed that estimate internal defect locations and sizes using surface defect measurements for hardwood logs [38]. Combining the external and internal defect information allows one to get a more complete understanding of log quality. More importantly, such data permit optimization of the sawing process to produce maximum value [39].

19.3 Physical, Mechanical, and Electrical Property-Based Techniques

19.3.1 Acoustic-Based Techniques

Techniques that employ acoustic wave propagation have been extensively researched for use as NDE tools. Speed and attenuation of induced acoustic waves in a material are frequently used as NDE parameters for assessing the mechanical properties of wood materials.

Much work in this area has been conducted, worldwide. For example, fundamental and applied studies have been conducted and reported on that examined the use of ultrasound to evaluate wood properties. A review on the use of ultrasound to assess wood has been prepared and published [40].

To illustrate acoustic wave techniques, consider application of one-dimensional wave theory to a homogeneous viscoelastic bar (Fig. 19.7). After an impact hits the end of the bar, a compression wave is generated that immediately begins moving down the bar as particles at the leading edge of the wave become excited, while particles at the trailing edge come to rest. The wave depth or the distance between the leading and trailing edges of the wave is controlled by the length of the impactor and the velocity of propagation of the

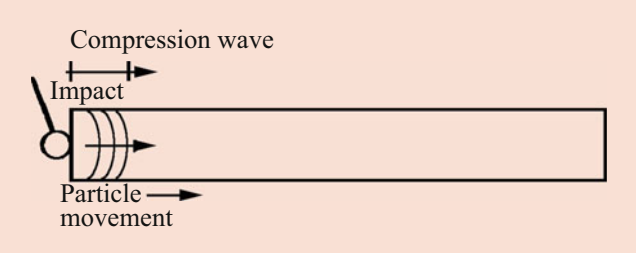

Fig. 19.7 Viscoelastic bar of length, l, subjected to an impact

Fig. 19.8 Travel of compression wave along bar. The forward-moving wave impinges on the free end of the bar, is reflected back as a tensile wave, and begins to travel back down the bar

material that makes up the impactor. The wave moves along the bar at a constant speed and its individual particles have only small longitudinal movements as a result of the wave passing over them. After traveling the length of the bar, this forward-moving wave impinges on the free end of the bar and is reflected as a tensile wave traveling back down the bar (Fig. 19.8). The velocity of the wave is independent of the intensity of the impact.

Energy is dissipated as the wave travels through the bar; therefore, although the speed of the wave remains constant, movement of particles diminishes with each successive passing of the wave. Eventually all particles of the bar come to rest. Monitoring the movement of a cross section near the end of such a bar in response to a propagating stress wave results in waveforms that consist of a series of equally spaced pulses whose magnitude decreases exponentially with time (Fig. 19.9).

The propagation speed C of such a stress wave can be determined by coupling measurements of the time between pulses, Δt, and the length of the bar L by

$$C = \frac{2L}{\Delta t} \tag{19.1}$$

The modulus of elasticity (MOE) can be computed using C and the mass density of the bar ρ:

$$\text{MOE} = C^2 \rho \tag{19.2}$$

Wave attenuation can be determined from the rate of decay of the amplitude of pulses using the following equation for logarithmic decrement:

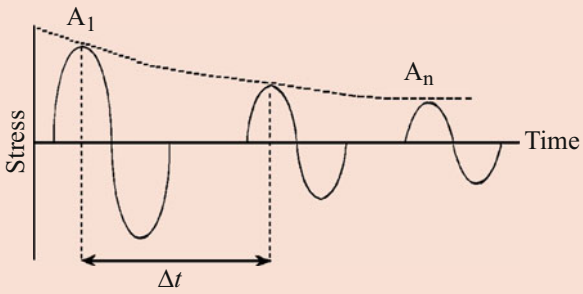

Fig. 19.9 Typical waveforms consist of a series of equally spaced pulses whose magnitude decreases exponentially with time

$$\delta = \frac{1}{(n-1)} \ln \frac{A_1}{A_n} \tag{19.3}$$

where A_1 and A_n are the amplitudes of two oscillations n–1 cycles apart (Fig. 19.9).

Note that wave attenuation calculated by this formula is highly dependent upon characteristics of the excitation system used. Thus, results reported by various researchers cannot be directly compared because several excitation systems were employed. Nonetheless, these results show that energy loss characteristics as measured by acoustic wave techniques provide useful information on the performance of wood-based materials.

A more rigorous treatise on the measurement of energy loss by acoustic wave techniques is presented by Kolsky [44]. In general, a more appropriate method for evaluating energy loss would be to determine the quantity of energy imparted into a member and the corresponding rate of energy loss. Loss of energy would be calculated using an integral of a waveform, as is done for determining the energy emitted during acoustic emission testing of materials [45].

Wood is neither homogeneous nor isotropic; therefore, the usefulness of one-dimensional wave theory for describing stress wave behavior in wood could be considered dubious. However, several researchers have explored application of the theory by examining actual waveforms resulting from propagating waves in wood and wood products and have found that one-dimensional wave theory is adequate for describing wave behavior. For example, Bertholf [46] found that the theory could be used to accurately predict dynamic strain patterns in small wood specimens. He verified predicted stress wave behavior with actual strain wave measurements as well as dependence of propagation velocity on the MOE of clear wood. Ross [47] examined wave behavior in both clear wood and wood-based composites and observed excellent agreement with one-dimensional theory. Similar results were obtained with clear sawn timber in tests conducted by Kaiserlik and Pellerin [48].

An interesting series of experiments designed to explore wave behavior in sawn timber was conducted by Gerhards

[49, 50]. He observed changes in the shape of a wave front in sawn timber containing knots and cross grain by measuring the change in wave speed in the vicinity of such defects. He concluded that a stress wave traveling in sawn timber containing knots and cross grain does not maintain a planar wave front.

One common technique that employs acoustic wave NDE techniques uses simple time-of-flight type measurement systems to determine wave propagation speed (Figs. 19.10 and 19.11). In these measurement systems, a mechanical or ultrasonic impact is used to impart a longitudinal wave into a member. Piezoelectric sensors are placed at two points on the member and used to sense passing of the wave. The time required for the wave to travel between sensors is measured and used to compute wave propagation speed.

Figure 19.12 illustrates a typical pulse echo test setup. An impact or "pulse" on one end of the specimen induces a wave to flow along the length of a specimen. The pulse is "echoed" from the opposite end of the specimen, hence the term pulse echo. Characteristics of waveforms observed when using the pulse echo technique are highly dependent upon the type of sensor used. Various types of sensors, including those that measure particle displacement, particle velocity, and particle acceleration or strain, can be used with this type of test setup. Figure 19.13 illustrates example waveforms obtained by transducers that measure particle velocity and acceleration. Note that the time required for a pulse to travel a round trip through the specimen can be obtained by using any of these transducers. The formula for transmission time is

$$\text{Transmission time} = \frac{\Delta t}{2L} \qquad (19.4)$$

where Δt is time between pulses and L is specimen length.

Note that this technique, as described, requires that both ends of the specimen are freely supported. A fixed end support condition will yield waveforms with different characteristics. Figure 19.14 illustrates a typical pitch and catch test setup. A pulse is introduced in the specimen, sensed by a transducer, and then allowed to flow through the specimen. The leading edge of the pulse is then sensed by a second transducer located further down the specimen. A pitch and catch test setup yields an electronic signal similar to that illustrated in Fig. 19.15. The time required for the wave or pulse to travel between the sensors can be calculated by the following equation:

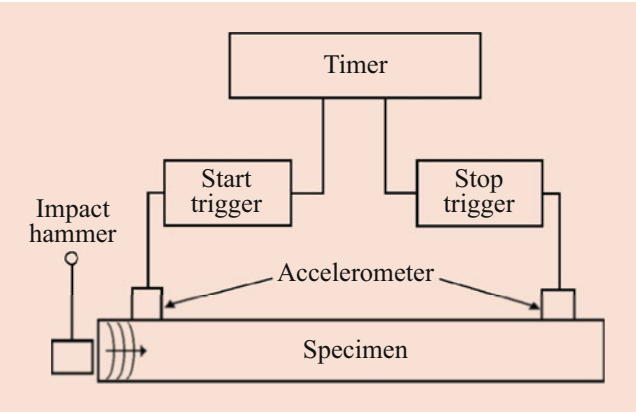

Fig. 19.10 System used to measure impact-induced stress wave propagation speed in wood

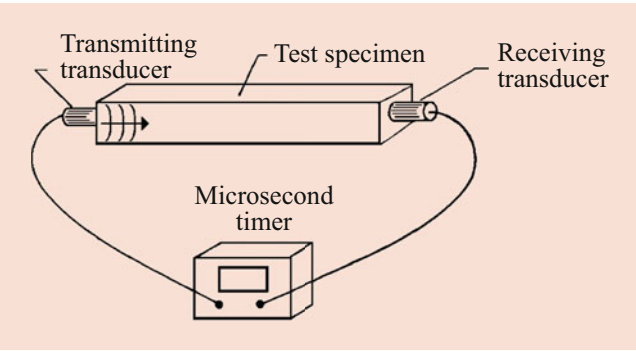

Fig. 19.11 System used to measure ultrasonic wave propagation speed in wood

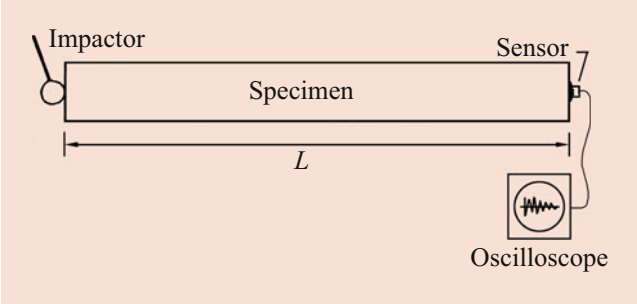

Fig. 19.12 Typical pulse echo test setup

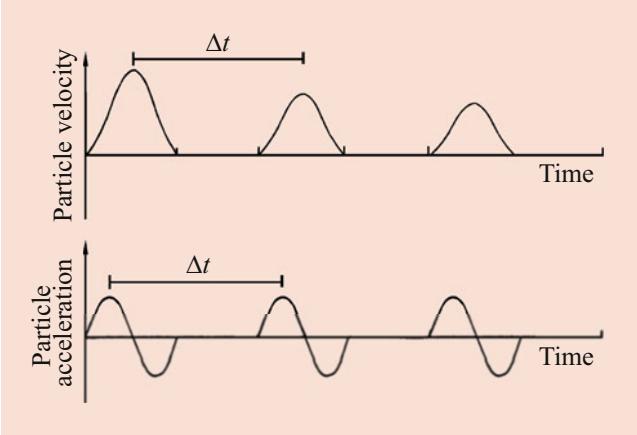

Fig. 19.13 Example waveforms obtained by transducers that measure particle velocity and acceleration

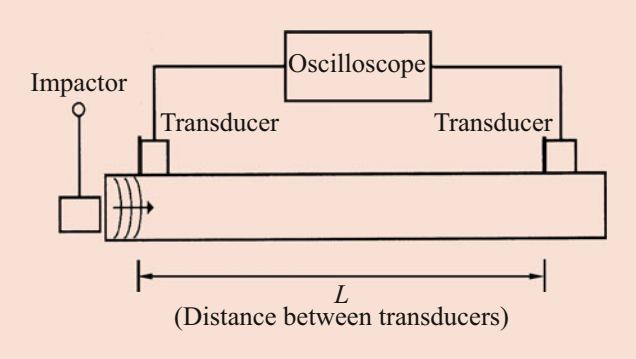

Fig. 19.14 Typical pitch and catch test setup. Pulse is introduced in specimen, sensed by transducer, and allowed to flow through specimen

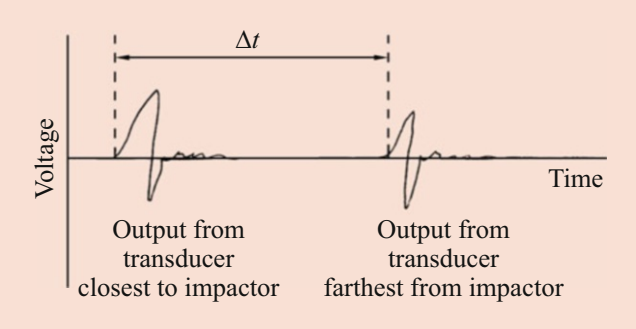

Fig. 19.15 Electronic signal yielded by pitch and catch test setup

$$\text{Transmission time} = \frac{\Delta t}{L} \qquad (19.5)$$

where Δt is time between pulses and L is distance between transducers.

Two key points should be considered when using the pitch and catch test setup: (1) the transducers must be in line with each other and (2) many transducers are sensitive to the manner in which they are installed. For example, commonly used accelerometers yield wave forms that are strongly dependent upon which direction they sense the pulse. Note that in Fig. 19.16, the base of the accelerometer directly faces an approaching compressive wave. Simply turning the accelerometer so that its base faces away from the approaching compressive wave changes the characteristics of the waveform.

Stress wave transmission times on a per length basis for various wood species are summarized in Table 19.1. Note that stress wave transmission times are shortest along the grain (parallel to fiber) and longest across the grain (perpendicular to fiber). Note that for Douglas-fir and Southern pine, stress wave transmission times parallel to the grain are approximately 200 μs/m. Stress wave transmission times perpendicular to the grain range from 850 to 1000 μs/m.

Several research projects have been conducted on the use of one-dimensional wave theory for assessing the MOE of

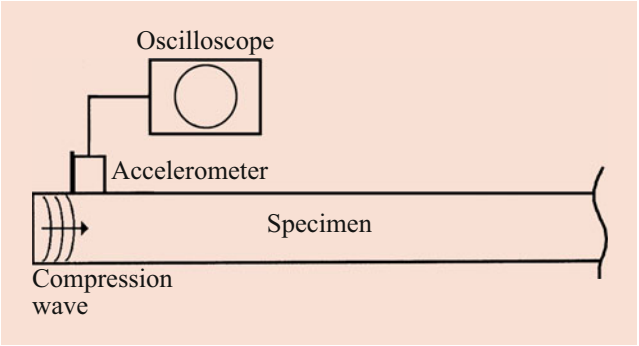

Fig. 19.16 Accelerometer positioned so that its base faces approaching compressive wave. Orientation of accelerometer influences characteristics of waveform

clear wood, lumber, and veneer. These studies have examined relationships between MOE values obtained from stress wave measurements and those obtained by static testing techniques. The strong correlative relationships found in these studies are shown in Table 19.2.

Table 19.3 summarizes research on the use of longitudinal acoustic wave techniques for assessing the strength properties of sawn timber and composite products. Kaiserlik and Pellerin [48], for example, used these techniques to evaluate the tensile strength of a small sample of clear sawn timber containing various degrees of slope of grain.

Extensive research has been conducted on the use of stress wave techniques for assessing the mechanical properties of wood composites [69–73]. Pellerin and Morschauser [69] showed that stress wave speed could be used to predict the flexural behavior of underlayment-grade particleboard. Ross [70] and Ross and Pellerin [71] showed that wave attenuation is sensitive to bonding characteristics and is a valuable NDE parameter that contributes significantly to the prediction of tensile and flexural mechanical behavior of wood-based particle composites. Vogt [73] examined the use of these techniques with wood-based fiber composites. In an additional study, Vogt [74] found a strong relationship between internal bond and wave parameters of particle and fiber composites.

The use of these techniques with wood subjected to different levels of biodeterioration, which adversely affects mechanical properties, initially focused on studies that employed only energy storage parameters (Table 19.4). For example, Pellerin et al. [60] showed that stress wave speed could be used to monitor the degradation of small, clear wood specimens exposed to brown-rot fungi. They showed a strong correlative relationship between wave speed and parallel-to-grain compressive strength of exposed wood. Rutherford et al. [57] showed similar results. These authors also revealed that MOE perpendicular to the grain, measured using stress wave NDE

Table 19.1 Summary of research on stress wave transmission times for various wood species

		Stress wave transmission time (μs/m)		
Reference	Species	Moisture content (% oven dry)	Parallel to grain	Perpendicular to grain
Smulski [51]	Sugar maple	12	256–194	–
	Yellow birch	11	230–180	–
	White ash Red oak	12 11	252–197 262–200	–
Armstrong et al. [43]	Birch Yellow-poplar Black cherry Red oak	4–6 4–6 4–6 4–6	213–174 194–174 207–184 226–177	715–676 15–676 689–620 646–571
Elvery and Nwokoye [52]	Several	11	203–167	–
Jung [53]	Red oak	12	302–226	–
Ihlseng [54, 55]	Several	–	272–190	–
Gerhards [56]	Sitka spruce Southern Pine	10 9	170 197	–
Gerhards [49]	Douglas-fir	10	203	–
Gerhards [50]	Southern Pine	10	197–194	–
Rutherford [57]	Douglas-fir	12	–	1092–623
Ross [58]	Douglas-fir	–	–	850–597
Hoyle and Pellerin [59]	Douglas-fir	9	–	1073
Pellerin et al. [60]	Southern Pine	9	200–170	613–1594
Soltis et al. [61]	Live oak	12	–	613–1594
Ross et al. [62]	Northern red and white oak	Green	–	795

Table 19.2 Summary of research on correlation between stress wave and static modulus of elasticity of clear wood, sawn timber, and veneer

Reference	Material	Static loading	Correlation coefficient r
Bell et al. [63]	Clear wood Clear wood	Compression Bending	0.98 0.98
Galligan and Courteau [64]	Clear wood Sawn timber	Bending	0.96
Gerhards [50]	Sawn timber Clear wood	Bending Bending	0.87 0.95
Koch and Woodson [65]	Veneer	Tension	0.96–0.94
McAlister [66]	Veneer	Tension	0.99
Porter et al. [67]	Sawn timber	Bending	0.90–0.92
Pellerin and Galligan [68]	Sawn timber Veneer	Bending Tension	0.96 0.96

techniques, was significantly affected by degradation from brown rot decay and could be used to detect incipient decay. Chudnoff et al. [75] reported similar results from experiments that utilized an ultrasonic measurement system and several hardwood and softwood species. Patton-Mallory and De Groot [77] reported encouraging results from a fundamental study dealing with the application of acousto-ultrasonic techniques. Their results showed that energy loss parameters may provide useful additional information on early strength loss from incipient decay caused by brown rot fungi. De Groot et al. [80] and Ross et al. [62, 81] used both energy storage and loss parameters to predict strength of deteriorated wood.

Verkasalo et al. [79] and Ross et al. [78] obtained encouraging results when using stress wave techniques to identify bacterially infected red oak. They found that speed of sound transmission perpendicular to the grain was significantly slower in sections of wood containing bacterial infection.

The use of acoustic-based techniques has been thoroughly researched as a tool for evaluating trees. A typical approach for measuring acoustic velocity in trees involves inserting two sensor probes (transmit probe and receiver probe) into the sapwood and introducing acoustic energy into the tree through a hammer impact on the transmit probe. The time-of-flight (TOF) is the time taken for the stress wave to travel from the transmit probe to the receiver probe. Acoustic velocity is subsequently calculated from

Table 19.3 Summary of results from studies using nondestructive stress wave testing techniques on sawn timber and wood composite products[a]

Reference	NDE technique	Material	NDE parameter measured	Static test	Reported properties	Comparison of NDE parameters and static properties (correlation coefficient *r*, unless noted)
Kaiserlik and Pellerin [48]	Longitudinal stress wave	Douglas-fir boards	C E_d, δ	Tension	UTS	UTS and E_d, 0.84; UTS and combination of E_d, δ, 0.90
Pellerin and Morschauser [69]	Longitudinal stress wave	Underlayment particleboard	C	Bending	E_{SB}, MOR	E_{SB}, and C^2, 0.93–0.95 MOR and C^2, 0.87–0.93
Ross [70], Ross and Pellerin [71]	Longitudinal stress wave	Underlayment and industrial particleboard, structural panel products	C, E_d, δ	Tension	E_{ST}, UTS	E_{ST} and C^2, 0.98 E_{ST} and E_d, 0.98 UTS and C^2, 0.91 UTS and E_d, 0.93 UTS and 1/δ, 0.63 UTS and combination of E_d, 1/δ, 0.95
Fagan and Bodig [72]	Longitudinal stress wave	Wide range of wood composites	C	Bending	MOR	Simulated and actual MOR distributions were similar.
Vogt [73]	Longitudinal stress wave	Medium-density fiberboard	C, E_d, δ	Tension	E_{ST}, UTS	E_{ST} and C^2, 0.90 E_{ST} and E_d, 0.88 UTS and C^2, 0.81 E_{SB}, and E_d, Combination, 0.88
		Underlayment and industrial particleboard		Bending	E_{SB}, MOR	E_{SB}, and C^2, 0.76 E_{SB}, and E_d, 0.72 MOR and C^2, 0.96 MOR and C^2, 10.92 Combination, 0.97
Vogt [74]	Stress wave (through transmission)	Underlayment and industrial particleboard, structural panel products	C_t, E_{dt}	Internal bond	IB	IB and C_t^2, 0.70–0.72 IB and E_{dt}, 0.80–0.99

[a]C speed of sound, C_t speed-of-sound transmission through thickness, δ logarithmic decrement, E_d dynamic modulus of elasticity (MOE) from transverse vibration or stress wave measurements, E_{dt} dynamic MOE through thickness orientation, E_{ST} MOE from static tension test, E_{SB} MOE from static bending test, *IB* internal bond, *MOR* modulus of rupture, *UTS* ultimate tensile stress

the span between the two sensor probes and the TOF measure using

$$C_T = \frac{S}{\Delta t} \tag{19.6}$$

where C_T is tree acoustic velocity (m/s), S is distance between the two probes (sensors) (m), and Δt is TOF.

During field acoustic measurement, the probes are inserted into the tree trunk (probes are inserted through bark and cambium to extend into the sapwood) and aligned within a vertical plane on the same face. The lower probe is placed about 40 to 60 cm above the ground. The span between the probes is determined from a practical standpoint, typically in the range 1.0–1.2 m; the probes need to be positioned at a comfortable height for the person who takes the measurements.

Acoustic velocities in logs and long stems of known length are typically measured using a pulse-echo based approach. In log acoustic measurement, an acoustic sensor is mounted or held on one end of a log. A stress wave is initiated by a mechanical impact on the same end, and the stress waveforms are subsequently recorded by an electronic unit. This acoustic approach is based on the observation of hundreds of acoustic pulses resonating longitudinally in a log and provides a weighted average acoustic velocity. Most resonance-based acoustic tools have a built-in fast Fourier transformation (FFT) program that can analyze and output the natural frequencies of the acoustic signals. Log acoustic velocity is then determined from

$$C_L = 2 f_0 L \tag{19.7}$$

where C_L is acoustic velocity of logs (m/s), f_0 is fundamental natural frequency of an acoustic wave signal (Hz), and L is log length (end-to-end) (m).

The resonance-based acoustic method is a well-established NDE technique for measuring long, slender wood members such as logs, poles, and timber [42, 82, 83]. The inherent accuracy and robustness of this method provide a significant advantage over TOF measurement in applications such as log measurement. In contrast to the TOF approach, the resonance method stimulates many, possibly hundreds, of acoustic pulse reverberations in a log, resulting in a very accurate and repeatable velocity measurement. Because of this accuracy, the acoustic velocity of logs obtained by the resonance-based measurement has served as a standard to validate the TOF measurement in standing trees [42, 84, 85].

Table 19.4 Research summary of correlation between nondestructive testing parameters and properties of degraded wood[a]

Reference	NDE technique	Material	Degradation agent	NDE parameter measured	Static test	Reported properties	Comparison of NDE parameters and static properties (correlation coefficient *r*, unless noted)
Chudnoff et al. [75]	Longitudinal stress wave (parallel to the grain)	Decayed and sound mine props; 26 species or species groupings	–	E_d	Compression parallel to grain	E_c, UCS	E_c and E_d, 0.84–0.97 (all species combined, hardwoods, maple, and oaks) E_c and E_d, 0.73–0.81 (all species, combined, southern pines, lodgepole pine) UCS and E_d, 0.85–0.95 (all species combined, hardwoods, maple, and oaks)
Pellerin et al. [60]	Longitudinal stress wave (parallel to the grain)	Small clear southern yellow pine specimens	Brown rot fungi (*Gloeophyllum trabeum*)	C, E_d	Compression parallel to grain	UCS	UCS and *C*: 0.47 (control) 0.73 (exposed) 0.80 (control and exposed) UCS and E_d, 0.86 (control) 0.86–0.89 (exposed) 0.94 (control and exposed)
			Termites (subterranean)	C, E_d			UCS and C: 0.65 (control) 0.21 (exposed) 0.28 (control and exposed) UCS and E_d: 0.90 (control) 0.79 (exposed) 0.80 (control and exposed)
Rutherford [76], Rutherford et al. [57]	Longitudinal stress wave (parallel to the grain)	Small, clear Douglas-fir specimens	Brown-rot fungi (*Gloeophyllum trabeum*)	C, E_d	Compression parallel to the grain	E_c, UCS	E_c and *C*, 0.91 E_c and E_d, 0.94 UCS and *C*, 0.67–0.70 UCS and E_d, 0.79 UCS and MOE, 0.80
Patton-Mallory and De Groot [77]	Longitudinal stress wave	Small, clear southern yellow pine specimens	Brown rot fungi (*Gloeophyllum trabeum*)	*C*, root mean square voltage frequency content of received signal	Bending	Maximum moment, alkali solubility	Linear decrease in *C* and decrease in strength with increased wood degradation. High-frequency components of signal attenuated in very early stages of decay
Ross et al. [78]	Longitudinal stress wave (parallel to the grain)	Red and white oak lumber	Bacteria (*Clostridium* and *Erwinia* sp.)	*C*	None	Presence of infection	Decrease in *C* with presence of infection
Verkasalo et al. [79]	Longitudinal stress wave (perpendicular to the grain)	Red oak lumber	Bacteria (*Clostridium* and *Erwinia* sp.)	*C*	Tension perpendicular to grain	UTS, presence of infection	Decrease in *C* and UTS with presence of infection

[a]*C* speed of sound, E_c modulus of elasticity (MOE) from static compression test, E_d dynamic MOE from stress wave measurements, *MOR* modulus of rupture, *UCS* ultimate compressive stress, *UTS* ultimate tensile stress

19.3.2 Transverse Vibration Methods

Transverse vibration techniques have received considerable attention for NDE applications. To illustrate these methods, an analogy can be drawn between the vibration of a mass that is attached to a weightless spring and internal damping force and the behavior of a vibrating beam (Fig. 19.17). In Fig. 19.17, mass *M* is supported from a rigid body by a weightless spring whose stiffness is denoted by *K*. Internal friction or damping is represented by the dashpot *D*. A

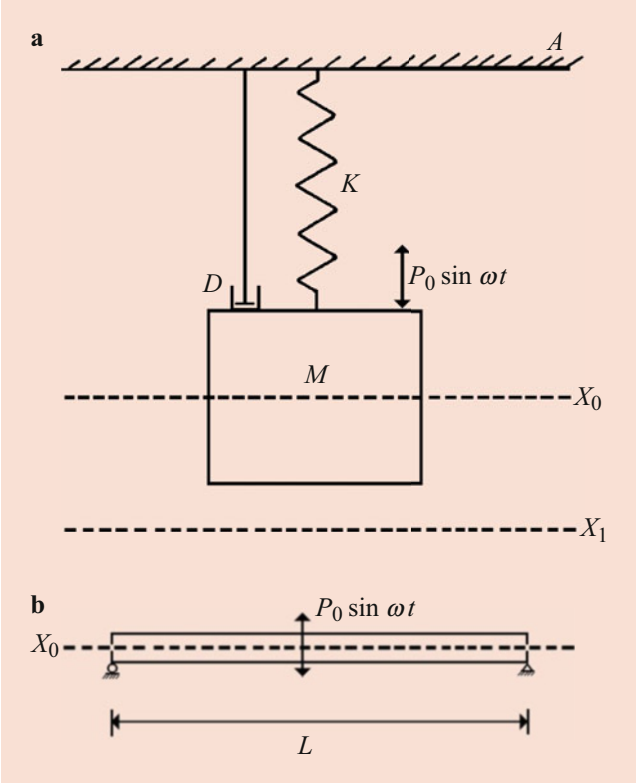

Fig. 19.17 Mass-spring dashpot vibration model (**a**) and transversely vibrating beam (**b**)

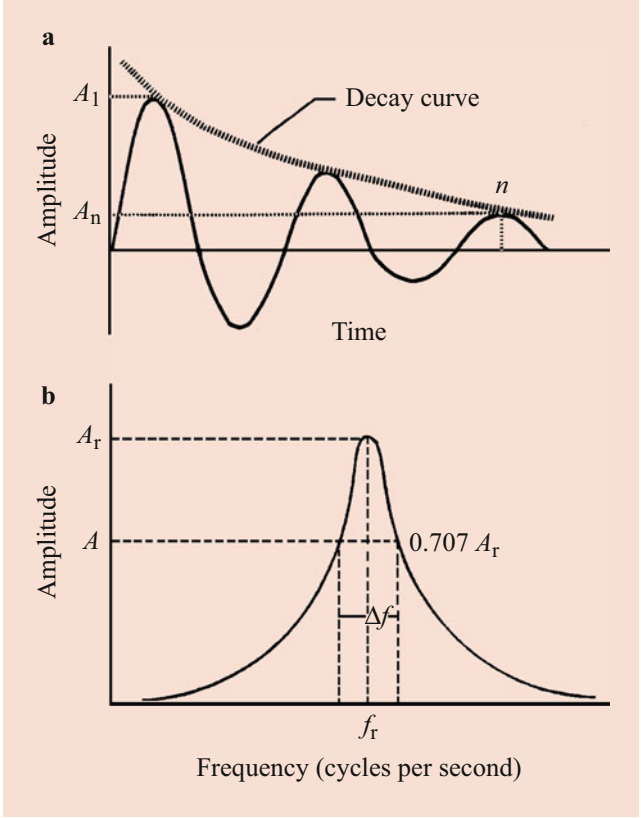

Fig. 19.18 Transverse vibration of a beam: (**a**) damped sine wave for a free vibration, (**b**) frequency response curve for a forced vibration

forcing function equaling $P_0 \sin \omega t$ or zero is applied for forced and free vibration, respectively. When M is set into vibration, its equation of motion can be expressed by

$$M\left(\frac{d^2x}{dt^2}\right) + D\left(\frac{dx}{dt}\right) + Kx = P_0 \sin \omega t \tag{19.8}$$

Equation (19.8) can be solved for either K or D. A solution for K will lead to an expression for MOE, where for a beam freely supported at two nodal points,

$$\text{MOE} = \frac{f_r^2 WL^3}{12.65Ig} \tag{19.9}$$

and for a beam simply supported at its ends,

$$\text{MOE} = \frac{f_r^2 WL^3}{2.46Ig} \tag{19.10}$$

In Eqs. (19.9) and (19–10.10), MOE is dynamic modulus of elasticity (Pa); f_r, resonant frequency (Hz); W, beam weight (kg); L, beam span (m); I, beam moment of inertia (m^4); and g acceleration due to gravity (9.81 m/s^2).

Solving Eq. (19.8) for D leads to an expression of the internal friction or damping component. The logarithmic decrement of vibrational decay is a measure of internal friction and can be expressed in the following form

For free vibrations,

$$\delta = \frac{1}{(n-1)} \ln \frac{A_1}{A_n} \tag{19.11}$$

where A_1 and A_n are the amplitudes of two oscillations n–1 cycles apart (Fig. 19.18).

For forced vibrations,

$$\delta = \frac{\pi \Delta f}{f_r} \frac{1}{\sqrt{\left(\frac{A_r}{A}\right)^2 - 1}} \tag{19.12}$$

where Δf is difference in frequency of two points of amplitude A on each side of a resonance curve, f_r is frequency at resonance, and A_r is amplitude at resonance (Fig. 19.18b).

Sharpness of resonance Q is frequently used to measure damping capacity; Q is defined as the ratio $f_r/\Delta f$. Note that if the value $0.707A_r$ (half-power point method) is substituted for A in Eq. (19.12), the equation reduces to

$$\delta = \frac{\pi \Delta f}{f_r} \tag{19.13}$$

and

$$Q = \frac{\pi}{\delta} \tag{19.14}$$

Table 19.5 summarizes research on the use of transverse vibration NDE techniques. Jayne [86] designed and conducted one of the first studies that used these techniques for evaluating the strength of wood. He was successful in demonstrating a relationship between energy storage and dissipation properties measured by forced transverse vibration techniques and the static bending properties of small clear wood specimens. Using a laboratory experimental setup, Jayne [86] was able to determine the resonant frequency of a specimen from a frequency response curve. In addition, sharpness of resonance (energy loss) was obtained using the half-power point method.

Pellerin [87, 88] used a similar experimental setup to examine the free transverse vibration characteristics of sawn timber and glulam. After obtaining a damped sine waveform for a specimen, he analyzed it using equations for MOE and logarithmic decrement. Measured values of MOE and logarithmic decrement were then compared to static MOE and strength values. O'Halloran [89] used a similar apparatus and obtained comparable results with softwood sawn timber. Wang et al. [90] used transverse vibration techniques to evaluate the static bending MOE of structural lumber. Ross et al. [91] obtained comparable results through coupling relatively inexpensive personal computer technologies and transverse vibration NDE techniques. Research on the use of transverse vibration techniques to assess the potential of hardwood sawn timber for structural applications is summarized in Table 19.6.

Proper procedures and important aspects for using transverse vibration testing techniques to evaluate MOE of wood-based flexural members are outlined in [41]. Three elements are essential when using this type of technique: the support apparatus, excitation system, and measurement system.

Support Apparatus

- The apparatus should provide vertical support to the ends of the specimen yet permit rotation
- The specimen should be supported so as to prevent damage at the point of contact between the specimen and the reaction support. The reactions should be such that shortening and rotation of the specimen about the reaction resulting from deflection are not restricted
- Provisions should be made at the reactions to allow for initial twist in the length of the specimen. If the bearing surfaces of the specimen at its reaction are not parallel, the specimen should be shimmed or the bearing surfaces rotated about an axis parallel to the span to provide adequate bearing across the width of the specimen

Table 19.5 Summary of research using transverse vibration nondestructive evaluation techniques[a]

Reference	NDE technique	Material	NDE parameter measured	Static test	Reported properties	Comparison of NDE parameters and properties (correlation coefficient *r*, unless noted)
Jayne [86] [b]	Forced transverse vibration	Small clear Sitka spruce specimens	Resonant frequency, E_d, Q	Bending	E_{SB}, MOR	E_{SB} and E_d, ± 690 MPa MOR and E_d, ± 6.9 MPa MOR and E_d, ± 6.9 MPa MOR and density/Q, ± 6.9 MPa MOR and E_d/δ, ± 6.2 MPa
Pellerin [87]	Free transverse vibration	Douglas-fir glulam	Natural frequency, E_d, δ	Bending	E_{SB}, MOR	Predicted relative strength of three glued-laminated members
Pellerin [88]	Free transverse vibration	Inland Douglas-fir dimension sawn-timber	Natural frequency, E_d, δ	Bending	E_{SB}, MOR	E_{SB} and E_d, 0.98 MOR and E_d, 0.67–0.93 MOR and 1/δ, 0.46–0.88 MOR and 1/δ, 0.68–0.92
O'Halloran [89]	Free transverse vibration	Lodgepole pine dimension sawn-timber	Natural frequency, E_d, δ	Bending	E_{SB}, MOR	E_{SB} and E_d, 0.98 MOR and E_d, 0.89 MOR and 1/δ, 0.82 MOR and E_d/δ, 0.91
Wang et al. [90]	Free transverse vibration	Spruce–Pine–Fir dimension sawn-timber	E_d	Bending	E_{SB}	E_{SB} and E_d, 0.96–0.99
Ross et al. [91]	Free transverse vibration	Spruce–Pine–Fir dimension sawn-timber	E_d	Bending	E_{SB}	E_d and E_{SB}, 0.99

[a] δ logarithmic decrement, E_d dynamic modulus of elasticity (MOE), E_{SB} MOE obtained from static bending test, *MOR* modulus of rupture, Q sharpness of resonance.
[b] Correlation coefficients were not reported by Jayne. However, he did report 95% confidence intervals

Table 19.6 Summary of research on the correlation between dynamic modulus of elasticity and other mechanical properties of hardwood sawn-timber[a]

Reference	Species group	Moisture content (%)	Grade[b]	Nominal width (mm)	Growth location	NDE technique	Static property	Correlation coefficient
Green and McDonald [92]	Northern red oak (*Quercus velutina, Q. rubra*)	12	1, 2, 3	100	Central Wisconsin	Transverse vibration (flatwise)	E_{SB}, UCS, UTS, MOR	E_{SB} and E_d, 0.92 MOR and E_d, 0.58 UTS and E_d, 0.54 UCS and E_d, 0.70 E_{SB} and E_d, 0.85
Green and McDonald [93]	Maple (*Acer rubra*)	12	SS, 2, 3	100	Central Vermont	Transverse vibration (flatwise)	E_{SB}, UCS, UTS, MOR	E_{SB} and E_d, 0.85 E_{SB} and E_d, 0.42 UTS and E_d, 0.46 UTS and E_d, 0.60

SS select structural

[a]E_d, dynamic modulus of elasticity (MOE) obtained from transverse vibration measurements; E_{SB}, MOE obtained from static bending test; MOR, modulus of rupture; UTS, ultimate tensile stress; UCS, ultimate compressive stress

[b]Grades by procedures given in the National Grading Rule performed by a quality supervisor of Southern Pine Inspection Bureau

- No lateral support should be applied. Specimens unstable in this mode should not be tested
- The specimen should be positioned such that an equal portion of the length overhangs each support. Excessive overhang may alter results. If Eq. (19.10) is used, the span to length (S/L) ratio of the specimen should be approximately 0.98. Other S/L ratios may be used, but a more exacting analysis and equation are needed. An overhang of approximately 25 mm on each end is often used in tests of sawn timber. The amount of overhang may be influenced by the convenience of handling and positioning, but it should be kept uniform from specimen to specimen

Excitation System

- The member should be excited so as to produce a vertical oscillation in a reproducible manner in the fundamental mode
- Manual deflection of the specimen will provide sufficient impetus for oscillation for many products. The deflection should be vertical with an effort to exclude lateral components; neither excessive impact nor prolonged contact with the specimen is recommended. For example, a manual tap on a 4.8 m, 38x86 mm piece of sawn timber with MOE of 13.8 GPa and supported flatwise will result in a vertical oscillation of 3 to 4 Hz
- Specimens with very high stiffness require mechanical excitation by a high force or carefully regulated impact/release

Measurement System

- Measurement of the frequency of oscillation should be obtained by either a force or displacement measuring device
- Changes in force in response to the vibration at one or both supports are used to obtain frequency of oscillation
- Frequency of oscillation can also be determined by measuring mid-span displacement in response to initial displacement
- It is critical that only the frequency associated with the fundamental vertical oscillation mode be used. Immediately after the specimen is excited, many vibration modes appear. The modes associated with higher frequencies than the fundamental bending frequency usually dissipate rapidly. Therefore, a short delay is necessary before acquiring the data to ensure that the data are related only to the fundamental vertical mode. This is an effective way to filter undesired modes from the data
- The span-to-depth ratio should be greater than 60 unless special precautions are taken to permit higher frequency measurements. With small span-to-depth ratios, it is difficult to verify that the specimen is oscillating in a bending mode. Best results are obtained when the frequency of oscillation is less than 30 Hz

In summary, it is important to note that this test method recommends transverse vibration testing of specimens in a flatwise orientation; this results in a relatively simple, low-frequency vertical vibration. Testing edgewise complicates the test because a specimen may vibrate in several modes, specifically vertically and horizontally, which could lead to erroneous results. Consequently, care should be taken when using these techniques for testing specimens in an edgewise orientation.

19.3.3 Static Bending Techniques

Measuring the MOE of a member by static bending methods is a relatively simple procedure that involves using the load–deflection relationship of a simply supported beam. Modulus

of elasticity can be computed directly by using equations derived from fundamental mechanics of materials.

Initial laboratory studies to verify the relationships between static bending methods and structural performance characteristics were conducted with sawn-timber products. Considerable research in the early 1960s examined the relationships between static bending test methods and the strength of softwood sawn timber. Summaries of various projects designed to examine this relationship are presented in Tables 19.7, 19.8, and 19.9. A wide range of sawn-timber products was evaluated, and the bending, compressive, and tensile strengths of the materials were investigated. In all cases, useful correlative relationships were discovered.

Some commercially available equipment uses static bending techniques to evaluate the MOE of structural sawn timber. For example, Metriguard, Inc. (Pullman, WA, USA), manufactures a range of products that utilize bending techniques to evaluate the flexural properties of structural sawn timber. A more detailed discussion of their high-speed production equipment is presented in Ross [6].

Figure 19.19 illustrates a typical center point loading test setup. The specimen is simply supported at both ends, a load is applied, and the mid-span deflection that results from the load is measured. MOE of the specimen is calculated as

$$\mathrm{MOE} = \frac{PL^3}{48I\delta} \tag{19.15}$$

where P is applied load (N), L is span (m), I is moment of inertia (m^4), and δ is mid-span deflection (m).

For this test setup, significant attention must be placed on design of the end supports. Ideally, the supports should be rigid so that no vertical displacement of the supports occurs. In addition, horizontal movement of the specimen on the end support should not be restricted, and the end supports need to be rotated and fixed to accommodate twist in the specimen.

19.3.4 Proof Loading – Concepts and History

Structural end jointing of sawn timber has become common practice, and high-strength end joints now permit the design of structures with long wood members that would not otherwise be considered feasible. Nevertheless, engineers and architects are often hampered in designing with wood because of the lack of complete quality assurance. If the structural integrity of an efficiently designed building were to rely upon any one member, the engineer would need to know without question that the member would withstand a minimum known level of stress indefinitely [109].

Although present sawn-timber stress grades assigned nondestructively have proven to be significantly more reliable than visually graded sawn timber, systems now in commercial use are insensitive to the quality of end joints – except in the case of extremely weak joints. Other methods of nondestructive evaluation of sawn timber have also proven to be

Table 19.7 Research on the correlation between modulus of elasticity (tested flatwise) and flatwise bending strength of softwood dimension sawn timber

Reference	Species	Moisture content (%)	Grade[a]	Nominal width (mm)	Growth location	Correlation coefficient r
Hoyle [94]	Douglas-fir	12	SS, C, U	100, 150, 250	Western Oregon, Washington, Idaho	0.79
					Washington	0.72
	Western hemlock	12	SS, C, U	100, 150, 250	Western Oregon, Washington	0.74
	Western larch	12	SS, C, U	100, 150, 200	Idaho, Washington	0.70
Hoyle [95]	Grand fir	12	C, S, U	200	Idaho	0.75
Hofstrand and Howe [96]	Grand fir	12	C, S	100, 150, 200	Idaho	0.75
Pellerin [97]	Douglas-fir	12	Combination of visual grades	100, 200	Idaho	0.76
Hoyle [98]	Southern pine	12	1D, 1, 2D, 2, 3	100, 150, 200	Southeastern United States	0.76
Kramer [99]	Southern pine	12	1D, 2, 3	100, 150, 250	Southeastern United States	0.88
Johnson [100]	Douglas-fir	10	SS, C, U	150	Western Oregon, Washington	0.85
	Western hemlock	10	SS, C, U	150	Western Oregon, Washington	0.86

[a]Grades are by regional rules in use at time of research. Western Products Association and West Coast Lumber Inspection Bureau Grades: *SS* Select Structural, *C* Construction, *S* Standard, *U* Utility. Western Wood Products Association Grades: 1, 2, 3. Southern Pine Inspection Bureau Grades: 1D, No. 1 Dense; 1, No. 1; 2D, No. 2 Dense; 2, No. 2; 3, No. 3

Table 19.8 Research on the correlation between modulus of elasticity (tested flatwise and on edge) and edgewise bending strength of softwood sawn timber

Reference	Species	Moisture content (%)	Grade[a]	Nominal width (mm)	Growth location	Correlation coefficient
Hoerber [101]	Douglas-fir	12	SS, C, U	100, 150, 200	Idaho, eastern Washington	0.65
Hoyle [95]	Grand fir	12	C, S, U, SS	200	Idaho	0.59–0.70
Hoyle [98]	Southern pine	12	1D, 1, 2D, 2, 3	100, 150, 200	Southeastern United States	0.57
Sunley and Hudson [102]	Norway spruce and Scots pine (pooled)	–	–	100, 180	Great Britain	0.68
Corder [103]	Douglas-fir	12	SS, C, S	100, 150, 250	Inland northwestern United States	0.64
Johnson [100]	Douglas-fir	10	SS, C, U	150	Western Oregon, Washington	0.80–0.87
	Western hemlock	10	SS, C, U	150	Western Oregon, Washington	0.86
Littleford [104]	Douglas-fir Western hemlock Noble fir Western white spruce Lodgepole pine	10 10 12 12 17	— — — — — —	150 150 150 150 150 150 150	British Columbia, Canada	0.74 0.70–0.77 0.66 0.79 0.80
Miller [105]	White spruce Jack pine	12 12	— —	150 150	Eastern Canada	0.78–0.84 0.69–0.73
Doyle and Markwardt [106]	Southern pine	12	1D, 1, 2D, 2, 3	100, 150, 200, 250	Southeastern United States	0.66
Hoyle [107]	Southern pine	12	1D, 1, 2D, 2, 3	100, 150, 250	Southeastern United States	0.67

[a]Grades are by regional rules in use at time of research. Western Products Association and West Coast Lumber Inspection Bureau Grades: *SS* Select Structural, *C* Construction, *S* Standard, *U* Utility. Western Wood Products Association Grades: 1, 2, 3. Southern pine Inspection Bureau Grades: lD, No. 1 Dense; 1, No. 1; 2D, No. 2 Dense; 2, No. 2; 3, No. 3

Table 19.9 Research on the correlation between modulus of elasticity (tested flatwise) and the compressive and tensile strength of softwood sawn timber

Strength property	Reference	Species	Moisture content (%)	Grade[a]	Nominal width (mm)	Growth location	Compression coefficient *r*
Compressive	Hofstrand and Howe [96]	Grand fir	12	Ungraded	100, 200	Idaho	0.84
	Pellerin [108]	Douglas-fir	12	SS, S, E	100, 200	Idaho	0.78
	Hoyle [107]	Southern pine	12	1, 2, 3	100, 200	Southeastern United States	0.67
Tensile	Hoyle [107]	Douglas-fir	15	1.0, 1.4, 1.8, 2.2	100, 200	Idaho	0.74
		White fir	14			Idaho	0.75
		Western hemlock	15			Western Oregon, Washington	0.81

[a]Grades are by regional rules in use at time of research. Western Products Association and West Coast Lumber Inspection Bureau Grades: *SS* Select Structural, *S* Standard, *E* Economy. Western Wood Products Association Grades: 1, 2, 3. Machine Stress Grades: 1.0, 1.4, 1.8, 2.2

unresponsive to end-joint properties. These methods include transverse vibration, acoustic-based, and microwave systems. Consequently, the remaining method that appears to offer potential for complete quality assurance for end joints is a proof load.

The principle of a proof-load system is that each end joint or complete member is stressed to the maximum of its design

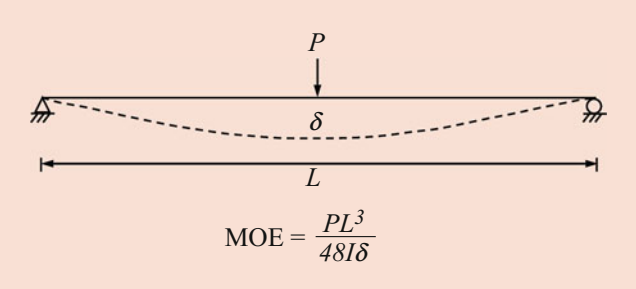

Fig. 19.19 Centerpoint loading test setup

limitation, times a factor, before the member is accepted for a critical-stress application. Pieces having characteristics, natural or otherwise, that preclude them from actually sustaining the intended working stress are fractured by the proof load and as a result are rejected. Proof loading, in a sense, serves to identify pieces of wood with superior strength properties that may then be used for higher design purposes. Consequently, in terms of structural integrity, much greater confidence can be placed in members that successfully withstand a proof load than in members that have not been subjected to proof loading [109].

Two stress modes for proof loading of end-jointed sawn timber have been researched: tension parallel to grain and flatwise bending [109–115].

In one of the first attempts to examine the concept of tension proof loading, scientists reasoned that the proof-load factor must be 2.1 (because the primary stress in the critical outside lamination of a beam was in tension) and that the minimum ultimate strength of the beam had to be 2.1 times the design stress.

The resultant strengths of beams fabricated from laminations that were proof loaded to a tensile stress of 2.1 times design stress are shown in Fig. 19.20. These results made it apparent that the proof-load factor could be lowered to near 1 and still result in adequate beam strengths. Table 19.10 shows how a single proof-load value could be used to evaluate many proof-load factors. For example, proof loading to approximately 20.7 MPa would result in a proof load factor of 1.4 for a design value of 15.2 MPa. After arriving at a proof-load factor of 1.4, another series of beams was fabricated. The resultant stress values (Fig. 19.21) show that the beams maintained the minimum allowable level.

The first commercial use of this tension proof-loading concept was in 1974 by Hood Industries in Laural, Mississippi, USA. The company realized the need for such a concept because of customer complaints about joint failures. The second commercial use was by St. Regis in Libby, Montana, USA.

The Hood Industries installation was out of line so that joints could adequately cure prior to proof loading, whereas the St. Regis in-line installation stresses the joints to the desired proof-load level after approximately 10 s out of the radiofrequency (RF) tunnel used to cure the adhesive in the joint.

A portable model of a tension proof-loading machine was developed for the American Institute of Timber Construction (AITC). This machine was air transportable in three packages. AITC used this machine to qualify their member plants for minimum tension-strength end-joints.

Subsequently, Suddarth [116] of Purdue University reported that strength performance of I-beams could be improved by a factor of 1.4 if built with tension proof loaded sawn timber.

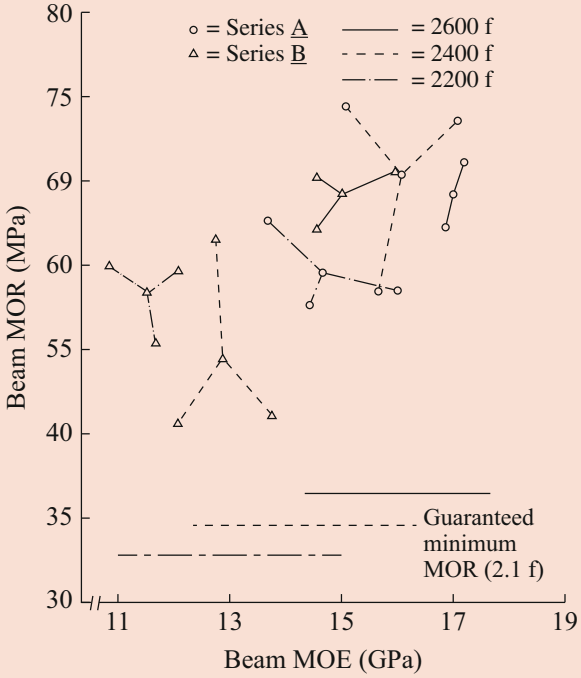

Fig. 19.20 Properties of laminated beams fabricated from laminations proof loaded to 2.1 times design stress

Table 19.10 Single proof-load value (MPa) used to evaluate many proof-load factors

	Proof-load factor				
f	1.0	1.1	1.2	1.3	1.4
13.8	13.8	15.2	16.6	17.9	19.3
15.2	15.2	16.7	20.8	19.7	21.3
16.6	16.6	18.2	19.9	21.5	23.2
17.9	17.9	19.7	21.5	23.3	25.1
19.3	19.3	21.3	23.2	25.1	27.0
20.7	20.7	22.8	24.8	26.9	29.0
22.8	22.8	25.0	27.3	29.5	31.9

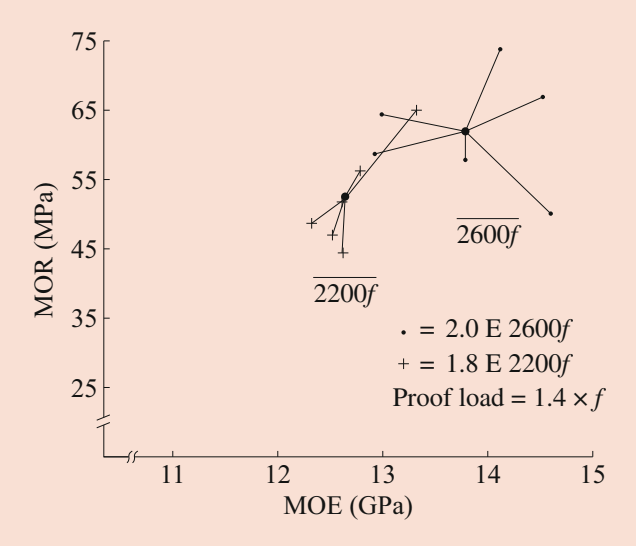

Fig. 19.21 Properties of laminated beam fabricated from laminations proof loaded to 1.4 times design stress

Although results of research on tension proof loading demonstrated that significant improvements in allowable design properties of laminated beams can be obtained from proof loading and that commercial machines have performed adequately, the laminating industry, through AITC, requested research on a bending proof-load concept.

The goals of a bending proof-load concept were to: 1) improve the reliability of glued-laminated timbers by eliminating the occasional low-strength end-joint; 2) eliminate the need for spacing end-joints within the beam when approved proof-loading procedures are followed; and 3) make it easier for glued-laminated timber to comply with reliability-based procedures when the need arises.

The immediate objective of this research was to develop data and criteria so that proof loading by bending could be incorporated into a laminating plant's production and quality control systems.

To achieve these goals and objectives, it was necessary to have information on the effects of proof loading on sawn timber, fully cured finger-joints, hot finger-joints, bending strength of fully cured joints that had been proof loaded while hot, tensile strength of fully cured joints that had been proof loaded while hot, and various configurations of finger-joints (including horizontal and vertical).

Table 19.11 shows average ultimate values for sawn timber stressed in bending, tension, and tension after being proof loaded in bending. The resulting proportion of ultimate tensile stress to ultimate bending stress for lumber is 60%. Typical data for finger-jointed sawn timber are summarized in Table 19.12. The resulting proportion of ultimate tensile stress to ultimate bending stress for sawn timber containing finger-joints is also 60%

Table 19.11 Average ultimate values for sawn timber stressed in bending, tension, and tension after being proof loaded in bending

Mode of test	Average ultimate stress (MPa)
Bending	63
Tension	37
Tension after 41 MPa bending proof load	37

Table 19.12 Average ultimate values for finger-jointed sawn timber stress in bending, tension, and tension after being proof loaded in bending

Mode of test	Average ultimate stress (MPa)
Bending	66
Tension	40
Tension after 41 MPa bending proof load	41

The objective of the second phase of the bending study was to determine the strength ratio of partially cured end joints to fully cured end joints. The procedure for this phase included the selection of a random sample of visually graded sawn timber for use in laminated beams designated as 301–24 Douglas-fir sawn timber from sources in southwest Oregon to northwest Washington. This sawn timber was used to make test specimens containing either a horizontal or a vertical finger-joint. Sixty matched pairs of specimens of each finger-joint orientation were subjected to two different procedures. In the first, the specimens were assembled, cured by RF energy, and allowed to fully cure. In the second, specimens were assembled, cured by RF, and tested to failure in bending within 10 s after the RF generator had shut off. The fully cured specimens were then tested to failure in bending at the same rate of loading used for the partially cured joints. Results are summarized in Table 19.13. Ratios of hot to cold strengths for both horizontal and vertical joints are reported in Table 19.14.

The objective of the third phase was to determine if bending proof loading of the hot joint affects final cold strength of the joints. Three more groups, 60 specimens each, of the vertical finger-joints were made. Two groups were proof loaded immediately out of the RF energy and then allowed to fully cure. The third group was assembled and allowed to fully cure without proof loading. Tensile strengths were determined for the group allowed to fully cure without proof loading and for one of the groups that had been proof loaded while hot.

Finally, a series of test beams were fabricated with the remaining group of laminations that had been proof loaded in bending for finger-joint quality assurance. The beams were laid up so that finger-joints in the three outermost tension

Table 19.13 Hot and cold ultimate bending stresses of both vertical and horizontal finger-joints and time to fail hot joints after removal from RF energy source

Type of joint	Joint condition	Average bending stress (MPa)	Time to failure (s)
Vertical	Hot Cold	36 67	7.27 —
Horizontal	Hot Cold	30 69	6.65 —

Table 19.14 Proportions of hot to cold ultimate bending stress for horizontal and vertical joints

Type of joint	Proportion (%)
Vertical	53
Horizontal	52

Table 19.15 Properties of beams fabricated from proof-loaded laminations and with stacked joints in the three outermost tension laminations

	Proof load		
Beam series	No. of laminations	Stress level (MPa)	Average ultimate stress (MPa)
1.8–1	2	18	39
1.8–2	3	18	45
2.2–1	2	25	45
2.2–2	2	27	48

laminations were stacked. The resulting beam properties are reported in Table 19.15.

Based on the results of this study and the commitment of AITC to proof loading, Mann-Russell Electronics (Tacoma, Washington) developed a bending-proof-loading machine for commercial application.

19.3.5 Piezoelectric Techniques

Piezoelectricity is the charge that accumulates in certain solid materials (notably crystals, certain ceramics, and biological matter such as bone and various proteins) in response to applied mechanical stress. Piezoelectricity means electricity resulting from pressure and is the direct result of the piezoelectric effect.

The piezoelectric effect is understood as the linear electromechanical interaction between mechanical and electrical states in crystalline materials. Piezoelectric effect is a reversible process in that materials that exhibit direct piezoelectric effect (the internal generation of electrical charge resulting from an applied mechanical force) also exhibit the reverse piezoelectric effect (internal generation of a mechanical strain resulting from an applied electrical field). For example, lead-zirconate-titanate crystals will generate measurable piezoelectricity when their static structure is deformed by about 0.1% of the original dimension. Conversely, those same crystals will change about 0.1% of their static dimension when an external electric field is applied to the material.

Piezoelectricity is found in useful applications such as the production and detection of sound, generation of high voltages, electronic frequency generation, microbalances, and ultrafine focusing of optical assemblies.

The electrical character of a piezoelectric material must be that of a dielectric wherein charge displacement far outweighs conduction. Thus, the material behaves according to the relationship: $C = Q/V$, where C is the capacitance (farads); Q, the charge (coulombs); and V, the potential difference (volts).

At the molecular level, a further requirement is placed on the piezoelectric material: There must be planes of molecular symmetry and within these planes the molecular constituents must be oriented in such a manner that the electrical charge centers are not symmetrically located. Monocrystals are representative of materials that meet these requirements.

When a piezoelectric crystal is strained, the charge centers are displaced relative to one another, causing a net charge to occur on the crystal surface. The dielectric nature of the crystal, obeying the capacitance relationship, permits the charge to appear as a voltage. This voltage is the electrical evidence of the piezoelectric effect.

The fundamental equations that describe the relationship between mechanical stress and electrical charge are

$$\begin{cases} P = dS + \eta E \\ \gamma = JS + dE \end{cases} \tag{19.16}$$

where a stress S is given to a substance, a polarization P is produced.

At the same time, an electric field E is also caused by the polarization of the substance. The coefficient d is called the piezoelectric modulus and η the electric susceptibility. The converse effect is shown by the second equation. A mechanical strain γ is produced by an applied electric field E and is accompanied by a stress S. The coefficient d for the converse effect is the same as that for the direct effect. If the condition is made that $E = 0$, then, by an experimental procedure, the modulus d can be determined as a ratio of polarization P to stress S.

Characteristics of piezoelectricity considered above apply directly to monocrystalline materials. Piezoelectricity of wood cannot be discussed easily in this context; although the same fundamental relations are believed to be applicable, it is necessary to consider the extremely heterogeneous nature of wood. Shubnikov [117] noted this fact in some of the first reported work on piezoelectricity of wood; he proposed the concept of "piezoelectric texture" to represent a system consisting of many crystalline particles oriented unidirectional.

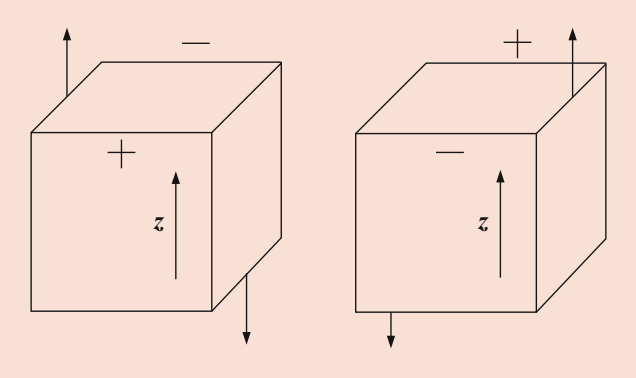

Fig. 19.22 General scheme to produce piezoelectric polarization in wood [118]

The piezoelectric effect in wood may be observed as illustrated in Fig. 19.22. The *z*-axis represents the fiber direction in wood. If a shearing stress is applied as indicated by arrows, an electrical polarization takes place in the direction perpendicular to the plane of the stress. The sign of the value of polarization is reversed when the direction of shear is reversed.

Rectangular coordinates are assigned to the wood structure with the *z*, *x*, and *y* axes representing the longitudinal, radial, and tangential directions in a tree trunk, respectively (Fig. 19.23).

It is known that cellulose is crystallized to a fairly large extent and that the unit cell of cellulose crystal belongs to monoclinic symmetry *C*2. The piezoelectric tensor for a crystal is determined by the symmetry of a crystal lattice [118].

The structure of wood composed of cellulose fiber is very complicated. Assume that the fiber is composed of many numbers of cellulose crystallites, orientated in the same direction as the fiber axis, and that such fibers are regularly orientated parallel to the trunk axis.

Cellulose fibrils twist spirally with a certain angle to the longitudinal axis of the cell. However, if the average is taken for the layers in which fibrils describe a spiral form in alternative directions, the form of the resultant tensor of piezoelectric modulus is the same as derived above.

Because polymeric substances possess a viscoelastic property, it is anticipated that when stress is applied, electrical polarization does not appear instantly but arises gradually with time. Therefore, the piezoelectric modulus is treated as a complex quantity and determines the phase lag between stress and polarization as well as the absolute value of the modulus.

Table 19.16 provides a summary of the species used in several reported studies. Note that a wide range of species has been used in these studies, and all have exhibited a piezoelectric effect. Reported moisture content values of the specimens used in the studies varied considerably, from a relatively dry state (below 10%) to over 70%. The specimens

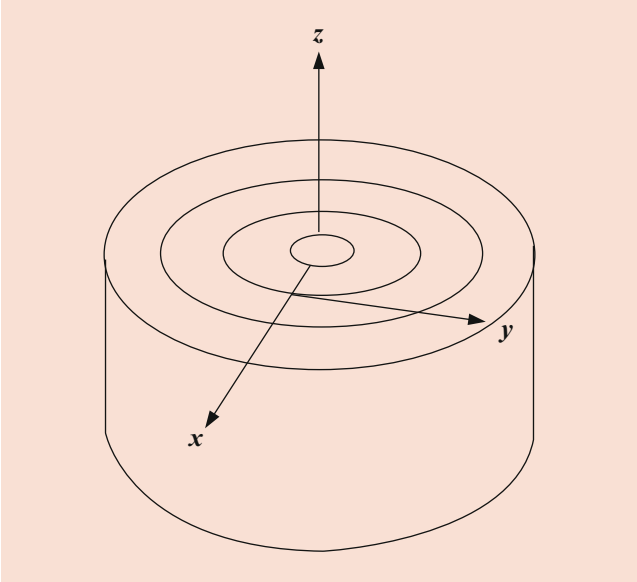

Fig. 19.23 Rectangular coordinates assigned to wood [118]

used were relatively small, with any dimension not exceeding 60 mm. Galligan and Courteau [64], Knuffel [127], and Knuffel and Pizzi [126] were exceptions – they used sawn-timber-size specimens in their experiments.

Most reported work used test setups that resulted in a uniform compressive stress being applied to the specimen, orienting each specimen so that the angle between growth rings and the application of load was approximately 45°. The electric charge generated was detected by electrodes that consisted of conductive paint, glued-on metal foil, pins, or small metal buttons placed against a specimen's surface.

Based on early experimentation by Bazhenov [134], Fukuda [135, 136], and Hirai et al. [123], the magnitude of the piezoelectric modulus of wood is approximately 1/20 that of a quartz crystal. Bazhenov [134] and Hirai et al. [123] found that the values of the piezoelectric modulus, d_{14}, increased gradually from the pith to the bark of a tree. They also reported that the values of the piezoelectric modulus for earlywood and latewood, for the same year's growth, were nearly equal.

Fukada et al. [120] found that the piezoelectric moduli increased with increasing density. Bazhenov [134] found that the piezoelectric modulus d_{25} increased and d_{14} decreased with increasing density in pines. Hirai et al. [121] confirmed that the d_{25} piezoelectric modulus increased with increasing density, but they show no data for d_{14}.

Bazhenov [134] found that the piezoelectric modulus is related to temperature, and it increases as temperature increases. Maeda et al. [128] found that d' of the piezoelectric constant of the Japanese cedar at 74% moisture content increased with increasing temperature for the piezoelectric constant determined at 10 Hz.

Table 19.16 A list of wood species investigated for piezoelectric effect in previous studies

Reference	Species
Fei and Zeng [119]	*Magnolia grandiflora* Linn *Tilia amurensis* Rupr *Taxodium* ascendens Brongn *Pinus massoniana* Lamb *Cunninghamia lanceolata* Hook
Fukada and others [120]	(10 old timbers from 8 years to 1300 years)
Galligan and Courteau [64]	Douglas-fir
Hirai and others [121, 122]	Tsuga (*Tsuga sieboldii* Carr.) Shioji (*Fraxinus mandshurica* Rupr.) Shirakaba (*Betula platyphylla* SUKATCHEV. var.; *japonica* HARA.) Hônoki (*Magnolia obovata* THUNB) Taiwanhinoki (*Chamaecyparis taiwanensis* MASAM. et SUZUKI) Kiri (*Paulownia tomentosa* STEUD.) Hinoki (*Chamaecyparis obtuse* ENDL.) Sugi (*Cryptomeria japonica* D. DON) Konara (*Quercus serrata* MURRAY.) Akamatsu I (*Pinus densiflora* SIEB. et ZUCC.) Akamatsu II Douglas-fir (*Pseudotsuga taxifolia* BRITT.) Makanba
Hirai and others [123]	Sugi (earlywood and latewood)
Hirai and others [124]	Hinoki tree (*Chamaecyparis obtuse* SIEB. et ZUCC)
Hirai and Yamaguchi [125]	Hinoki
Knuffel and Pizzi [126]	*Pinus patula*
Knuffel [127]	*Pinus patula* *Pinus taeda* *Pinus elliottii*
Maeda and others [128]	Japanese cedar
Nakai and Takemura [129]	Beisugi (*Thuja plicata* Donn) Hinoki (*Chamaecyparis obtuse* ((S. and Z.)) Endl.) Beitsuga (*Tsuga heterophylla* ((Raf.)) Sarg.) Beimatsu (*Pseudotsuga menziesii* ((Mirb.)) Franco) Buna (*Fagus crenata* Bl.)
Nakai and others [130]	Sitka spruce (*Picea sitchensis* Carr.)
Nakai and others [131]	Japanese cypress (*Chamaecyparis obtuse* Endl.)
Suzuki and others [132]	Hinoki (*Chamaecyparis obtuse* ((S. and Z.)) Endl.) Beimatsu (*Pseudotsuga menziesii* ((Mirb.)) Franco) Beihiba (*Chamaecyparis nootkatensis* ((D. Don)) Spach) Agathis (*Agathis* sp.) Igem (*Podocarpus imbricatus* Bl.) Momi (*Abies firm* S. and Z.) White fir (*Abies alba* Mill.) Spruce (*Picea pungens* Engelm) Shinanoki (*Tilia japonica* Simk) Katsura (*Cercidiphyllum japonicum* S. and Z.) Buna (*Fagus crenata* Bl.) Lauan (*Pentacme contorta* Merr. and Rolfe) Nato (*Palaquium* sp.) Matoa (*Pometia pinnata* Forst.) Sugar maple (*Acer saccharum* Marsh.)
Suzuki and Hirai [133]	*Chamaecyparis botusa* Endlicher *Larix leptolepis* Gordon *Magnolia ovobata* Thunberg

Smittakorn and Heyliger [137] developed a theoretical model for the steady-state and transient behavior of adaptive wood composite plates composed of layers of wood and other piezoelectric materials to simultaneously study the effects of mechanical, electrical, temperature, and moisture fields. They considered the theoretical model as a means of studying any laminated wood plate where the elastic, temperature, moisture, and electric fields influence the overall structural response. Their results of studying a representative example provided an indication of the level of response of adaptive

wood composites, although no experimental verification had been conducted in their investigation.

Fukada [135] and Bazhenov [134] both hypothesized that the piezoelectric effect observed in wood originates in crystalline cellulose regions of the cell wall and that its intensity is dependent upon the degree of crystallinity. Hirai et al. [123] furthered that hypothesis, postulating that the magnitude of the piezoelectric modulus of wood depend upon degree of crystallinity and orientation of cellulose crystals in the cell wall.

Using conformational analysis, Pizzi and Eaton [138] concluded that van der Waal forces were responsible for the piezoelectric effect in wood. They concluded that the electrical charge most likely develops in response to an imposed shear force that results in laminar lateral–longitudinal deformations in the five-strand unit of the crystalline cellulose I molecule found in the microfibrils of wood. They also concluded that electrostatic and hydrogen bond interactions do not contribute to the piezoelectric effect.

Hirai et al. [122, 124] showed that the piezoelectric modulus can be increased by increasing the crystallinity of the cellulose by treatment with gamma rays, exposure to high temperature for extended periods, liquid ammonia, ethylenediamine, or sodium hydroxide. Fukada et al. [120] found that aging wood increased its crystallinity and its piezoelectric modulus. Based on his experimental results, he also postulated that fungal decomposition decreased both crystallinity and piezoelectric modulus.

Nakai et al. [131] found that the first and second peaks in the piezoelectric voltage appeared almost simultaneously with the peak of the ratio of crystal lattice strain to surface strain. They also noted that the piezoelectric response decreased because of the effect of microscopic cracks in their specimens.

Nakai et al. [130] measured the piezoelectricity of kiln-dried Sitka spruce specimens and simultaneously recorded scanning-electron-microscope images in real time to observe the deformation process of wood. Results of their experiments showed that there were two types of microscopic destruction in the specimens. With the first type, although a small uprush around the boundary of the annual ring was observed, the specimens were broken only by shearing fracture in the 45° direction. With the second type, the specimens were finally broken by shearing fracture after repeated buckling. They found that the piezoelectric voltage increased almost linearly in the elastic region, proceeded to the maximal point, and then decreased gradually, and a clear peak appeared in the bucking and shearing fracture.

Nakai and Takemura [129] measured the piezoelectricity of air-dried specimens (from five species) under time-varying load to investigate the possible relationship between piezoelectricity and the fracture of wood. A time-varying load was applied at a constant rate, accompanying a preliminary load and a sinusoidal load with a frequency of 20 Hz. They found that the greatest voltage of the piezoelectric signals as reported in a previous paper was in the case of a grain angle of 45°, and the voltages of the piezoelectric signals depended on the magnitude of the load, species, and grain angle. The results of their experiments showed that the piezoelectricity–time curves can be classified into three types (type A, B, and C). Each curve consists of an initial rising part, a gradually increasing part, a subsequent decreasing part, and finally, a rapid rising and falling (type A and B) or merely falling part (type C), where the second part of the type B is much flatter compared with that of the type A. They also found that decreasing piezoelectricity against an increasing load was another characteristic behavior in the plastic region before a sudden fracture of a specimen.

Fukada et al. [120] found that the relation between the dynamic Young's modulus and the piezoelectric constant of the old timbers was linear (Fig. 19.24). Nakai et al. [130] reported a similar linear relation in the kiln-dried Sitka spruce with the exact relationship between the dynamic Young's modulus and the piezoelectric constant as:

$$E_c\left(\times\frac{10^3\mathrm{kg}f}{\mathrm{cm}^2}\right)=1.18\left(\frac{P_p}{\rho L_p}\right)+3.15 \qquad (19.17)$$

Hirai et al. [121] found that the piezoelectric effect varied with the angle between the direction of the stress and the direction of the fiber axis and that maximum piezoelectric polarization was obtained when the direction of the stresses were at angles of 45° and 135° with the direction of the fiber axis (Fig. 19.25).

Knuffel and Pizzi [126] measured the piezoelectric effect in *Pinus patula* structural timber beams. They found that the piezoelectric signal usually began smaller, increased to maximum after about five cycles, and then began to attenuate to

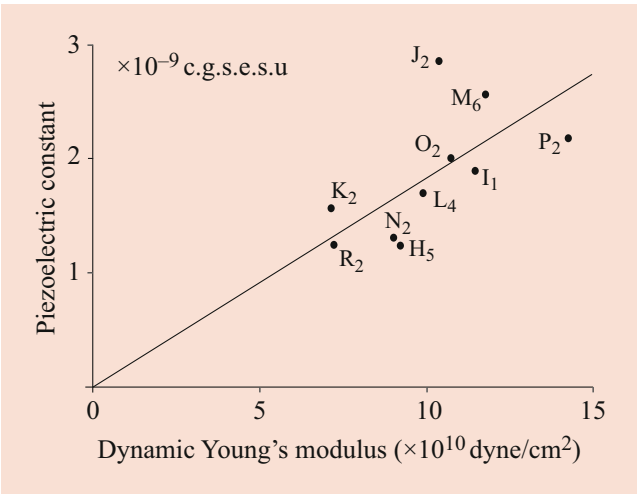

Fig. 19.24 The relation between dynamic Young's modulus and the piezoelectric constants of old timbers [120]

zero. Also, the piezoelectric response started to develop almost simultaneously with the arrival of the stress wave and reached its first peak within 0.0001 s. They observed that the first peak of the piezoelectric signals might be either positive or negative, which are uncontaminated by resonance. They also found that the piezoelectric effect in the wet sawn timber was still found to be very strong. However, because of the conductive conditions, the electrical signal originating at the beginning of the sawn timber propagated faster than the stress wave, and at 20% moisture content, the piezoelectric effect began to coincide with the arrival of the stress wave.

Knuffel [127] investigated the effect of the natural defects on the piezoelectric effect in structural timber. There were three findings from that investigation. First, the piezoelectric first wave peak values showed a definite and very sensitive increase in amplitude in the vicinity of knots and cross-grain (Fig. 19.26). Second, the piezoelectric response was far more sensitive to the defects than to MOE. Third, the piezoelectric effect was directly related to strain concentrations in the anatomical structure.

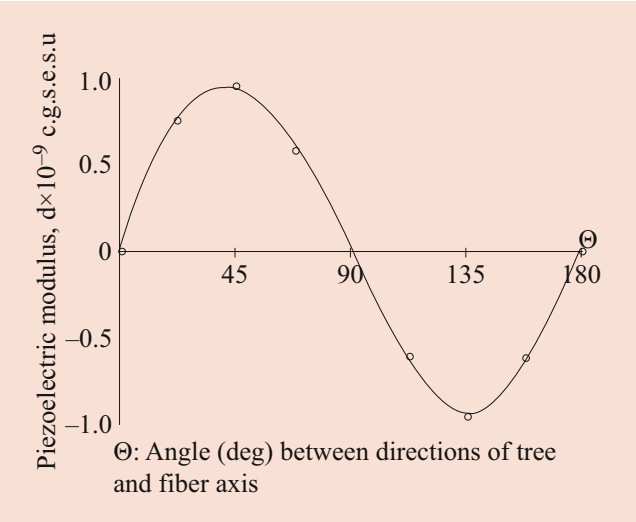

Fig. 19.25 Anisotropy of piezoelectric modulus [121]

19.3.6 Dielectric Permittivity

A nondestructive method for measuring the grain direction is based on the difference in dielectric constant (permittivity) of wood between the parallel direction (lower dielectric constant) and perpendicular (higher) to the grain. The dielectric constant is simply the ability of a material to concentrate an applied electric field. Measuring a material's dielectric constant can be as simple as measuring the current flow between two conductors with an alternating voltage applied. At low moisture-content levels, wood can be considered a dielectric material [139, 140, 141, 142]. The dielectric constant of a nonconducting material determines the amount of electric

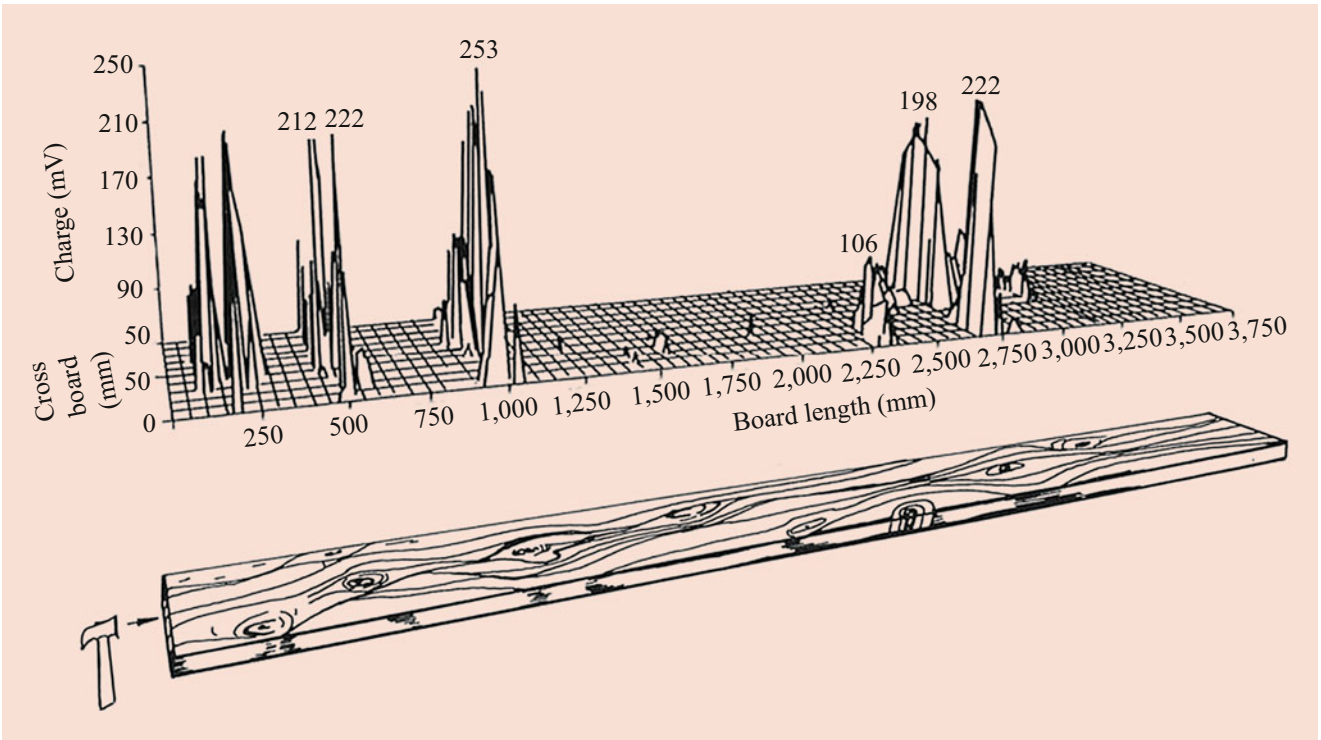

Fig. 19.26 Piezoelectric response in structural timber [127]

potential energy that is stored in a given volume of the material within an electric field. It is expressed as the ratio of the dielectric permittivity of the material relative to that of a vacuum or dry air. Experimentally it is determined as the ratio of the capacity of a condenser with the material acting as the dielectric relative to the capacity of the condenser when the space between the plates is dry air. The dielectric constant for wood varies with grain (fiber) direction, and commercial equipment has been developed that utilizes this fact to determine fiber orientation in wood products. It has been reported that knots, spiral grain, and other defects can be detected by measuring dielectric properties [143].

One commercially available piece of equipment (Metriguard Model 511 Grain Angle Meter) measures grain angle in wood as the direction of maximum dielectric permittivity projected onto a flat surface of the wood relative to a reference direction. This equipment consists of a stationary detector, operating controls, digital display, and USB port integrated into a handheld unit. The detector causes RF fields to be applied to the wood through defined areas on the wood surface and senses the field at another area on the wood surface. The sensed signal is amplified and processed to determine grain angle.

This nondestructive test method is currently being examined as a potential compliment to currently used techniques for evaluating the tensile properties of structural lumber.

References

1. Newman, P.C.: Caesars of the Wilderness: Company of Adventures, vol. 2, p. 450. Viking Adult, Markham (1987)
2. Ross, R.J., Wang, X.: International Nondestructive Testing and Evaluation of Wood Symposium Series. General Technical Report. FPL-GTR-213, p. 6,702. U.S. Department of Agriculture, Forest Service, Forest Products Laboratory, Madison (2012)
3. Ross, R.J. and X. Wang. 2013. Proceedings, 18th International Nondestructive Testing and Evaluation of Wood Symposium. General Technical Report. FPL-GTR-226. Madison: U.S. Department of Agriculture, Forest Service, Forest Products Laboratory: 808
4. Ross, R.J., Wang, X., Goncalves, R., R.: Proceedings, 19th International Nondestructive Testing and Evaluation of Wood Symposium. General Technical Report. FPL-GTR-239, p. 688. U.S. Department of Agriculture, Forest Service, Forest Products Laboratory, Madison (2015)
5. Wang, X., Senalik, C.A., Ross, R.J.: Proceedings, 20th International Nondestructive Testing and Evaluation of Wood Symposium. General Technical Report. FPL-GTR-246, p. 539. U.S. Department of Agriculture, Forest Service, Forest Products Laboratory, Madison (2017)
6. Ross, R.J.: Nondestructive Evaluation of Wood. Second Edition. General Technical Report. FPL-GTR-238, p. 167. U.S. Department of Agriculture, Forest Service, Forest Products Laboratory, Madison (2015)
7. So, C.-L., others: Forest Prod. J. **54**(3), 7–16 (2004)
8. Schimleck, L.R., Evans, R.: IAWA J. **23**(3), 217–224 (2002)
9. Schimleck, L.R., Evans, R., Ilic, J.: Can. J. For. Res. **31**(10), 1671–1674 (2001)
10. Meder, R., Thumm, A., Marston, D.: J. Near Infrared Spectrosc. **11**(5-6), 137–143 (2003)
11. Meglen, R.R. and Kelley, S.S.: Use of a region of the visible and near infrared spectrum to predict mechanical properties of wet wood and standing trees. US Patent No. 6,525,319 (2003a)
12. Meglen, R.R. and S.S. Kelley.: Method for predicting dry mechanical properties from wet wood and standing trees. US Patent No. 6,606,568 (2003b)
13. Meder, R., Thumm, A., Bier, H.: Holz als Roh-und Werkstoff. **60**(3), 159–164 (2002)
14. Kelley, S.S., Jellison, J., Goodell, B.: FEMS Microbiol. Lett. **209**(1), 107–111 (2002)
15. Hedrick, S.F., Bennett, R.M., Kelley, S.S., Rials, T.G.: In: Proc. ASCE/SEI 2004 Structures Congress, Nashville, TN. ASCE, Reston (2003)
16. Kelley, S.S.: Method for predicting mechanical properties of decayed wood. US Patent No. **6**, 593,572 (2003)
17. Wang, X., Wacker, J.P., Rammer, D.R.: In: Proceedings WCTE 2006: 9th World Conference on Timber Engineering, August 6-10, 2006, p. 5. Oregon State University, Portland, OR.: program and abstracts. (2006)
18. Brunner, C.C., Shaw, G.B., Butler, D.A., Funck, J.W.: Wood Fiber Sci. **22**(4), 413–428 (1990)
19. Conners, R.W., McMillan, C.W., Lin, K., Vasques-Espinosa, R.E.: IEEE Trans. Pattern Anal. Mach. Intell. **5**(6), 573–583 (1983)
20. Conners, R.W., C.W. McMillan, R.E. Vasques-Espinosa. 1984. In: Proceedings, 7th International Conference on Pattern Recognition, Montreal 7(1):416-419
21. Conners, R.W., McMillan, C.W., Ng, C.N.: In: Proceedings, First International Conference on Scanning Technology in Sawmilling, pp. XVIII-1–XVIII-33. Miller Freeman Publications, San Francisco (1985)
22. Forrer, J.B., Butler, D.A., Funck, J.W., Brunner, C.C.: Forest Prod. J. **38**(11/12), 75–79 (1988)
23. Forrer, J.B., Butler, D.A., Brunner, C.C., Funck, J.W.: Forest Prod. J. **39**(1), 39–42 (1989)
24. Brunner, C.C., Maristany, G.A.G., Butler, D.A., VanLeeuwen, D., Funck, J.W.: Ind. Metrol. **2**, 169–184 (1992)
25. Conners, R.W., Kline, D.E., Araman, P.A., Drayer, T.H.: Computer. **30**(7), 43–48 (1997)
26. Kline, D.E., Conners, R.W, Lu, Q., Araman, P.A.: In: Hardwood Symposium Proceedings, May 7-10, 1997. pp. 161–166 (1997)
27. Srikanteswara, S., Q. Lu, W. King, T. Drayer, R. Conners, E. Kline, P. Araman. 1997. In: Proceedings of SPIE, Machine Vision Applications, Architectures, and Systems Integration VI. October 15-16, 1997. Pittsburgh, PA. pp. 170-179
28. Thomas, R.E.: Chapter 9. Laser scanning of logs and lumber. In: Ross (ed.) Nondestructive evaluation of wood (second edition). General Technical Report FPL-GTR-238, pp. 103–107. U.S. Department of Agriculture, Forest Service, Forest Products Laboratory, Madison (2015)
29. Abbott, A.L., Schmoldt, D.L., Aeaman, P.A., Lee, S.-M.: In: Proceedings of Scan Tech International Conference, November 4-6, 2001, Seattle, WA, pp. 101–110. Wood Machining Institute, Berkeley, CA (2001)
30. Nyström, J.: Comput. Electron. Agric. **41**(2003), 91–99 (2003)
31. Åstrand, E.: Automatic Inspection of Sawn Wood. Ph.D. Thesis, No. 424. Linköping University, Sweden (1996)
32. Hansson, Å., A. Pettersson.: STFIs on-line barkmätare. Svensk papperstidning, Nordisk cellulose, in Swedish, pp. 32-33 (1993)
33. Jolma, I.P., Mäkyen, A.J.: In: Proceedings, SPIC 7022. Advanced Laser Technologies 2007, 70220G (2007)
34. Nyström, J.: Image based methods for nondestructive detection of compression wood in sawn timber. In: Licentiate Thesis 1999, 34. Luleå University of Technology, Sweden (1999)

35. Thomas, R.E., Thomas, L., Shaffer, C.: In: Proceedings of the 15th International Symposium on Nondestructive Testing of Wood, September 10-12, 2007, pp. 163–167. University of Minnesota Duluth, Duluth (2008)
36. Thomas, L., Thomas, R.E.: In: Fei, S., Lhotka, J.M., Stringer, J.W., Gottschalk, K.W., Miller, G.W. (eds.) Proceedings, 17th central hardwood forest conference; 2010 April 5-7; Lexington, KY; Gen. Tech. Rep. NRS-P-78, pp. 92–101. U.S. Department of Agriculture, Forest Service, Northern Research Station, Newtown Square (2011)
37. Hanks, L.F., Gammon, G.L., Brisbin, R.L., Rast, E.D.: Hardwood Log Grades and Lumber Grade Yields for Factory Grade Lumber Logs. Forest Service Res. Pap. NE-468, p. 92. Broomall, U.S. Department of Agriculture, Forest Service, Northeastern Research Station (1980)
38. Thomas, R.E.: Equations for predicting internal defect measurements of common Appalachian hardwoods. Res. Pap. FPL-RP-686, p. 16. U.S. Department of Agriculture, Forest Service, Forest Products Laboratory, Madison (2016)
39. Lin, W., Wang, J., Thomas, R.E.: In: Proceedings of the 17th Central Hardwoods Forest Conference, April 5–7, 2010, Lexington, KY. Gen. Tech.Rep. P-78, pp. 67–75. U.S. Department of Agriculture, Forest Service, Northern Research Station, Newtown Square (2011)
40. Senalik, C.A., Schueneman, G., Ross, R.J.: Ultrasonic-based nondestructive evaluation methods for wood: a primer and historical review. In: General Technical Report FPL-GTR-235, p. 31. U.S. Department of Agriculture, Forest Service, Forest Products Laboratory, Madison (2014)
41. American Society for Testing and Materials (ASTM): Standard Test Methods for Nondestructive Evaluation of Wood-Based Flexural Members Using Transversal Vibration. ASTM D 6874-12. American Society for Testing and Materials, Philadelphia (2012)
42. Andrews, M: In: Proceedings, 13th International Symposium on Nondestructive Testing of Wood. August 19–21, 2002, pp. 156–165. University of California, Berkeley (2003)
43. Armstrong, J.P., Patterson, D.W., Sneckenberger, J.E.: Wood Fiber Sci. **23**(1), 32–43 (1991)
44. Kolsky, H.: Stress Waves in Solids. Dover Publications, Inc, New York (1963)
45. Harris, D.O., Tetleman, A.S., Darwish, F.A.I.: Detection of Fiber Cracking by Acoustic Emission. Acoustic Emission. ASTM 505, p. 11. American Society for Testing and Materials, Philadelphia, PA (1972)
46. Bertholf, L.D.: Use of Elementary Stress Wave Theory for Prediction of Dynamic Strain in Wood. Bull. 291. Washington State University, College of Engineering, Pullman (1965)
47. Ross, R.J.: In: Proceedings, Fifth Nondestructive Testing of Wood Symposium; 1985 September 9–11; Pullman, WA, pp. 291–318. Washington State University, Pullman (1985)
48. Kaiserlik, J.H., Pellerin, R.F.: For. Prod. J. **27**(6), 39–43 (1977)
49. Gerhards, C.C.: Effect of Cross Grain on Stress Waves in Lumber. Res. Pap. FPL–RP–368. U.S. Department of Agriculture, Forest Service, Forest Products Laboratory, Madison (1980)
50. Gerhards, C.C.: Effect of Knots on Stress Waves in Lumber. Res. Paper FPL–RP–384. U.S. Department of Agriculture, Forest Service, Forest Products Laboratory, Madison (1982)
51. Smulski, S.J.: Wood Fiber Sci. **23**(1), 44–57 (1991)
52. Elvery, R.H., Nwokoye, D.N.: In: Proceedings, Paper II, Nondestructive Testing of Concrete and Timber, Organized by the Institution of Civil Engineering and the British Commission for Nondestructive Testing; 1969 June 11–12, pp. 105–110. Institute of Civil Engineering, London, BC (1970)
53. Jung, J.: Stress Wave Grading Techniques on Veneer Sheets. Gen. Tech. Rep. FPL–GTR–27. U.S. Department of Agriculture, Forest Service, Forest Products Laboratory, Madison (1979)
54. Ihlseng, M.C.: Van Nostrand's Eng. Mag. **XIX**, 8–9 (1878)
55. Ihlseng, M.C.: Am. J. Sci. 3d Series. **17**(98), 125–133 (1879)
56. Gerhards, C.C.: Wood Sci. **11**(2), 69–72 (1978)
57. Rutherford, P.S., Hoyle, R.J., De Groot, R.C., Pellerin, R.F.: In: Proceedings, 6th nondestructive testing of wood symposium; 1987 September 14–16, pp. 67–80. Washington State University, Pullman (1987)
58. Ross, R.J.: Quality Assessment of the Wooden Beams and Columns of Bay C of the East End of Washington State University's Football Stadium. Unpublished Research. Washington State University, Pullman (1982)
59. Hoyle, R.J., Pellerin, R.F.: In: Proceedings, Fourth Symposium on Nondestructive Testing of Wood. 1978 August 28-30; Vancouver, WA, pp. 33–45. Washington State University, Pullman (1978)
60. Pellerin, R.F., De Groot, R.C., Esenther, G.R.: In: Proceedings, 5th Nondestructive Testing of Wood Symposium; 1985 September 9–11; Pullman, WA, pp. 319–353. Washington State University, Pullman (1985)
61. Soltis, L; Baker. A.; Ferge, L. et al.: USS Constitution—inspection and evaluation procedures for live and white oak members. Report submitted to U.S. Navy, Maintenance and Repair, USS Constitution, Boston Naval Shipyard, Charlestown, MA (1992)
62. Ross, R.J., De Groot, R.C., Nelson, W.J.: Exp. Tech. **18**(5), 29–32 (1994)
63. Bell, E.R., Peck, E.C., Krueger, N.T.: Modulus of Elasticity of Wood Determined by Dynamic Methods. Rep. 1977. U.S. Department of Agriculture, Forest Service, Forest Products Laboratory, Madison (1954)
64. Galligan, W.L., Courteau, R.W.: In: Galligan, W.L. (ed.) Proceedings, Second Symposium on Nondestructive Testing of Wood. April, 1965, pp. 223–224. Washington State University, Spokane (1965)
65. Koch, P., Woodson, G.E.: For. Prod. J. **18**(10), 45–51 (1968)
66. McAlister, R.H.: For. Prod. J. **26**(10), 37–40 (1976)
67. Porter, A.W.; Kusec, D.J.; Olson, S.L. 1972. Digital computer for determining modulus of elasticity of structural lumber. WFPL Info. Rep. VP–X–99. Vancouver: Department of Environment, Canadian Forest Service
68. Pellerin, R.F.; Galligan, W.L.: Nondestructive method of grading wood materials. Canadian Patent 918286 (1973)
69. Pellerin, R.F., Morschauser, C.R.: In: Proceedings, 7th international particleboard symposium; 1973 March; Pullman, WA. - Washington State University, Pullman (1974)
70. Ross, R.J.: Stress Wave Speed and Attenuation as Predictors of the Tensile and Flexural Properties of Wood-Based Particle Composites. Washington State University, Pullman (1984) Ph.D. dissertation
71. Ross, R.J., Pellerin, R.F.: For. Prod. J. **38**(5), 39–45 (1988)
72. Fagan, G.B., Bodig, J.: In: Proceedings, Fifth Nondestructive Testing of Wood Symposium; 1985 September 9–11; Pullman, WA, pp. 3–37. Washington State University, Pullman, WA (1985)
73. Vogt, J.J.: Evaluation of the Tensile and Flexural Properties and Internal Bond of Medium Density Fiberboard Using Stress Wave Speed and Attenuation. Washington State University, Pullman (1985) M.S. thesis
74. Vogt, J.J.: In: Proceedings, 12th International Particleboard/Composite Materials Symposium; 1986 March; Pullman, WA. - Washington State University, Pullman (1986)
75. Chudnoff, M., Eslyn, W.E., McKeever, D.B.: For. Prod. J. **34**(3), 43–50 (1984)
76. Rutherford, P.S.: Nondestructive Stress Wave Measurement of Incipient Decay in Douglas Fir. Washington State University, Pullman (1987) M.S. thesis
77. Patton-Mallory, M., De Groot, R.C.: In: Proceedings, 2nd Pacific timber engineering conference; 1989 August 28–29. Auckland, New Zealand (1989)
78. Ross, R.J., Ward, J.C., TenWolde, A.: Identifying bacterially infected oak by stress wave nondestructive evaluation. Res. Pap.

FPL–RP–512. U.S. Department of Agriculture, Forest Service, Forest Products Laboratory, Madison (1992)
79. Verkasalo, E., Ross, R.J., TenWole, A., Youngs, R.L.: Properties Related to Drying Defects in Red Oak Wetwood. Res. Pap. FPL–RP–516. U.S. Department of Agriculture, Forest Service, Forest Products Laboratory, Madison (1993)
80. De Groot, R.C., Ross, R.J., Nelson, W.J.: In: Proceedings, Twenty Sixth Annual Meeting. IRG, Helsinger (1995). June 11-16, 1995
81. Ross, R.J., De Groot, R.C., Nelson, W.J., Lebow, P.K.: In: Sjostrom, C. (ed.) Proceedings, Seventh International Symposium on Durability of Building Materials and Components, Volume 1, pp. 637–644. E&FN Spon, 2-6 Boundary Row, London (1996)
82. Harris, P., Petherick, R., Andrews, M.: In: Proceedings, 13th International Symposium on Nondestructive Testing of Wood. August 19-21, 2002, pp. 195–201. University of California, Berkeley (2003)
83. Wang, X., Ross, R.J., Brashaw, B.K., Punches, J., Erickson, J.R., Forsman, J.W., Pellerin, R.F.: Wood Fiber Sci. **36**(3), 368–377 (2004)
84. Carter, P., Briggs, D., Ross, R.J., Wang, X.: Acoustic Testing to Enhance Western Forest Values and Meet Customer Wood Quality Needs. PNW–GTR–642. Productivity of Western Forests: a Forest Products Focus, pp. 121–129. USDA Forest Service, Pacific Northwest Research Station, Portland (2005)
85. Wang, X., Ross, R.J., McClellan, M., Barbour, R.J., Erickson, J.R., Forsman, J.W., McGinnis, G.D.: Wood Fiber Sci. **33**(4), 522–533 (2001)
86. Jayne, B.A.: For. Prod. J. **9**(11), 413–416 (1959)
87. Pellerin, R.F.: In: Proceedings, Second Nondestructive Testing of Wood Symposium; 1965 April; Spokane, WA, pp. 337–347. Washington State University, Pullman (1965a)
88. Pellerin, R.F.: For. Prod. J. **15**(3), 93–101 (1965b)
89. O'Halloran, M.R.: Nondestructive Parameters for Lodgepole Pine Dimension Lumber. Colorado State University, Fort Collins, CO (1969) M.S. thesis
90. Wang, Z., Ross, R.J., Murphy, J.F.: Wood For. Res. **6**(4), 86–88 (1993) (In Chinese)
91. Ross, R.J., Geske, E.A., Larson, G.L., Murphy, J.F.: Transverse vibration nondestructive testing using a personal computer. Res. Pap. FPL–RP–502. U.S. Department of Agriculture, Forest Service, Forest Products Laboratory, Madison (1991)
92. Green, D.W., McDonald, K.A.: Wood Fiber Sci. **25**(1), 35–45 (1993a)
93. Green, D.W., McDonald, K.A.: Wood Fiber Sci. **25**(4), 365–374 (1993b)
94. Hoyle, R.J.: For. Prod. J. **11**(6), 251–254 (1961)
95. Hoyle, R.J.: Analysis of Relationship between Stiffness and Strength of 2″ x 8″ White Fir (Abies Grandis) Used as Joist and Plank. Potlatch Forests, Inc, Lewiston (1962)
96. Hofstrand, A.D., Howe, J.P.: Relationship between Modulus of Elasticity and Compression Strength of White Fir. Potlatch Forests, Inc, Lewiston (1963)
97. Pellerin, R.F.: Correlation of strength properties of 1-inch lumber. In: Washington State University, Division of Industrial Research. Potlatch Forests, Inc., Lewiston (1963b)
98. Hoyle, R.J.: Research Results on Machine Stress Rated Southern Pine Lumber. Potlatch Forests, Inc, Lewiston (1964)
99. Kramer, P.R.: For. Prod. J. **14**(10), 495–496 (1964)
100. Johnson, J.W.: In: Proceedings, Second Nondestructive Testing of Wood Symposium; 1965 April; Spokane, WA, pp. 419–457. Washington State University, Pullman, WA (1965)
101. Hoerber, G.F.: A Study of Modulus of Elasticity and Modulus of Rupture in Douglas-Fir Dimension Lumber. Potlatch Forests, Inc, Lewiston (1962)
102. Sunley, J.G., Hudson, W.M.: For. Prod. J. **14**(4), 155–158 (1964)
103. Corder, S.E.: In: Proceedings, Second Nondestructive Testing of Wood Symposium; 1965 April; Spokane, WA, pp. 461–472. Washington State University, Pullman (1965)
104. Littleford, T.W.: In: Pullman, W.A. (ed.) Proceedings, Second Nondestructive Testing of Wood Symposium; 1965 April; Spokane, WA, pp. 475–485. Washington State University (1965)
105. Miller, D.G.: Proceedings, Second Nondestructive Testing of Wood Symposium. 1965 April, pp. 485–491. Washington State University, Spokane, Washington. Pullman: Washington (1965)
106. Doyle, D.V., Markwardt, L.J.: Properties of Southern Pine in Relation to Strength Grading of Dimension Lumber. Res. Pap. FPL–RP–64. U.S. Department of Agriculture, Forest Service, Forest Products Laboratory, Madison (1966)
107. Hoyle, R.J.: For. Prod. J. **18**(4), 87–97 (1968)
108. Pellerin, R.F.: Compression parallel to grain versus modulus of elasticity for Douglas-fir dimension lumber. In: Washington State University, Division of Industrial Research. Potlatch Forest, Inc., Lewiston (1963a)
109. Strickler, M.D., Pellerin, R.F., Talbott, J.W.: For. Prod. J. **20**(2), 29–35 (1970)
110. Pellerin, R.F., Strickler, M.D.: For. Prod. J. **21**(5), 50–55 (1971)
111. Pellerin, R.F., Strickler, M.D.: For. Prod. J. **22**(10), 24–30 (1972)
112. Pellerin, R.F., Strickler, M.D.: S. J. Struct. Div. Am. Soc. Chem. Eng. **103**(ST1), 270–274 (1977)
113. Strickler, M.D., Pellerin, R.F.: For. Prod. J. **21**(6), 19–24 (1971)
114. Strickler, M.D., Pellerin, R.F.: For. Prod. J. **23**(10), 34–36 (1973)
115. Strickler, M.D., Pellerin, R.F.: J. Struct. Div. Am. Soc. Chem. Eng. **102**(ST3), 645–657 (1976)
116. Suddarth, S.K.: In: Proceedings, 5th Symposium on Nondestructive Testing of Wood; 1985 September 9–11; Pullman, WA, pp. 549–559. Washington State University, Pullman, WA (1985)
117. Shubnikov, A.V.: Moskova, Russia: Izvestiya Akademii Nauk, Seriya Biologicheskaya [Proceedings of the Academy of Sciences, Biological Series]. 84 p. In Russian (1946)
118. Fukada, E.: Wood Sci. Technol. **2**, 299–307 (1968)
119. Fei, Y.Y., Zeng, S.X.: J. Nanjing For. Univ. **3**, 100–104 (1987)
120. Fukada, E., Yasuda, S., Kohara, J., Okamoto, H.: Oyo Butsuri. **26**, 25–28 (1957)
121. Hirai, N., Date, M., Fukada, E.: Mokuzai Gakkaishi. **14**(5), 247–251 (1968a)
122. Hirai, N., Date, M., Fukada, E.: Mokuzai Gakkaishi. **14**(5), 252–256 (1968b)
123. Hirai, N., Asano, I., Sobue, N., Naito, H.: Mokuzai Gakkaishi. **16**(7), 310–318 (1970)
124. Hirai, N., Sobue, N., Asano, I.: Mokuzai Gakkaishi. **18**(11), 535–542 (1972)
125. Hirai, N., Yamaguchi, A.: Mokuzai Gakkaishi. **25**(1), 1–6 (1979)
126. Knuffel, W., Pizzi, A.: Holzforschung. **40**(3), 157–162 (1986)
127. Knuffel, W.: Holzforschung. **42**(4), 247–252 (1988)
128. Maeda, H., Tsuda, H., Fukuda, E.: Rep. Prog. Polym.Phys. Japan. **20**, 739–742 (1977)
129. Nakai, T., Takemura, T.: Mokuzai Gakkaishi. **39**(3), 265–270 (1993)
130. Nakai, T., Igushi, N., Ando, K.: J. Wood Sci. **44**, 28–34 (1998)
131. Nakai, T., Yamamoto, H., Nakao, T., Hamatake, M.: Wood Sci. Technol. **39**, 163–168 (2005)
132. Suzuki, Y., Hirai, N., Ikeda, M.: **38**(1), 20–28 (1992)
133. Suzuki, Y., Hirai, N.: **42**(3), 271–280 (1995)
134. Bazhenov, V.A.: Piezoelectric Properties of Wood, p. 176. Consultants Bureau, New York (1961)
135. Fukada, E.: J. Phys. Soc. Jpn. **10**(2), 149–154 (1955)
136. Fukada, E.: In: Galligan, W.L. (ed.) Proceedings, Second Symposium on Nondestructive Testing of Wood. April, 1965, pp. 143–170. Washington State University, Spokane, WA (1965)
137. Smittakorn, W., Heyliger, P.R.: Wood Fiber Sci. **33**(4), 595–608 (2001)

138. Pizzi, A., Eaton, N.: Holzforschung und Holzverwertung. **36**(1), 12–14 (1984)
139. James, W.L., Hamill, D.W.: For. Prod. J. **15**(2), 51–56 (1965)
140. Kellog, R.M.: Physical properties of wood. In: Wangaard, F.F. (ed.) Wood: its Structure and Properties. Clark C. Heritage Memorial Series on Wood, Vol. 1, pp. 195–223. The Pennsylvania State University, University Park (1981)
141. Lin, R.T.: For. Prod. J. **17**(7), 61–66 (1967)
142. Skaar, C.: The dielectric properties of wood at several radio frequencies. NY State College of Forestry Technical Publication No. **69** (1948)
143. Martin, P., Collet, R., Barthelemy, P., Roussy, G.: Wood Sci. Technol. **21**, 361–371 (1987)

Prof. Dr. Robert J. Ross is a project leader at the USDA Forest Service, Forest Products Laboratory (FPL). His current research focus is the development and use of nondestructive evaluation technologies for various wood products and structures. He served as team leader and editor of the Centennial Edition of the Wood Handbook—Wood as an Engineering Material, FPL's flagship publication. In addition to his assignment at FPL, he is a research professor at Michigan Technological University and holds adjunct faculty appointments at Beijing Forestry University and Mississippi State University. He holds BS (Wood and Fiber Utilization) and MS (Engineering Mechanics) degrees from Michigan Technological University and a PhD in Engineering Science from Washington State University.

Dr. Xiping Wang received his PhD in Wood Science from Michigan Technological University in 1999. He is a Research Forest Products Technologist at the USDA Forest Service, Forest Products Laboratory (FPL), and the Associate Editor of the Journal of Materials in Civil Engineering (ASCE). His research focuses on nondestructive testing and evaluation of wood, condition assessment of wood structures, and urban tree hazard assessment.

Res.Eng. Christopher Adam Senalik is a Research General Engineer with the USDA Forest Service, Forest Products Laboratory (FPL). His areas of focus while at FPL have been nondestructive testing of wood, analysis of timber bridge structures, and moisture cycling effects on the strength of wood composites. He is currently involved in evaluating the use of ground-penetrating radar as an inspection tool for wood structures. He received his PhD in the area nondestructive evaluation of wood products from the University of Illinois, Urbana-Champaign. Prior to receiving his PhD, he was a forensic accident investigator specializing in heavy vehicle collisions.